

NASA TECHNICAL NOTE



NASA TN D-6813

c. 1

NASA TN D-6813

LOAN COPY: RETURN
AFWL (DOUL)
KIRTLAND AFB, N

01337237



TECH LIBRARY KAFB, NM

AIRCRAFT TIRE BEHAVIOR DURING HIGH-SPEED OPERATIONS IN SOIL

by Trafford J. W. Leland and Eunice G. Smith

Langley Research Center

Hampton, Va. 23365



NATIONAL AERONAUTICS AND SPACE ADMINISTRATION • WASHINGTON, D. C. • AUGUST 1972



0133737

1. Report No. NASA TN D-6813	2. Government Accession No.	3. Recipient's Catalog No.	
4. Title and Subtitle AIRCRAFT TIRE BEHAVIOR DURING HIGH-SPEED OPERATIONS IN SOIL		5. Report Date August 1972	6. Performing Organization Code
7. Author(s) Trafford J. W. Leland and Eunice G. Smith		8. Performing Organization Report No. L-7641	
9. Performing Organization Name and Address NASA Langley Research Center Hampton, Va. 23365		10. Work Unit No. 133-61-12-01	
12. Sponsoring Agency Name and Address National Aeronautics and Space Administration Washington, D.C. 20546		11. Contract or Grant No.	
15. Supplementary Notes		13. Type of Report and Period Covered Technical Note	
16. Abstract An investigation to determine aircraft tire behavior and operating problems in soil of different characteristics was conducted at the Langley landing-loads track with a 29 x 11.0-10, 8-ply-rating, type III tire. Four clay test beds of different moisture content and one sand test bed were used to explore the effects on axle drag loads developed during operation at different tire inflation pressures in free rolling, locked-wheel braking, and yawed (cornering) modes, all at forward speeds up to 95 knots. The test results indicated a complicated drag-load-velocity relationship, with a peak in the drag-load curve occurring near 40 knots for most test conditions. The magnitude of this peak was found to vary with tire inflation pressure and soil character and, in certain cases, might prove large enough to make take-off hazardous.		14. Sponsoring Agency Code	
17. Key Words (Suggested by Author(s)) Aircraft tires Unprepared runway operations Drag coefficients in soil Braking and cornering in soil		18. Distribution Statement Unclassified - Unlimited	
19. Security Classif. (of this report) Unclassified	20. Security Classif. (of this page) Unclassified	21. No. of Pages 62	22. Price* \$3.00

AIRCRAFT TIRE BEHAVIOR DURING HIGH-SPEED OPERATIONS IN SOIL

By Trafford J. W. Leland and Eunice G. Smith
Langley Research Center

SUMMARY

An investigation to determine aircraft tire behavior and operating problems in soil of different characteristics was conducted at the Langley landing-loads track with a $29 \times 11.0-10$, 8-ply-rating, type III tire. Four clay test beds of different moisture content and one sand test bed were used to explore the effects on axle drag loads developed during operation at different tire inflation pressures in free rolling, locked-wheel braking, and yawed (cornering) modes, all at forward speeds up to 95 knots. The test results indicated a complicated drag-load—velocity relationship, with a peak in the drag-load curve occurring near 40 knots for most test conditions. The magnitude of this peak was found to vary with tire inflation pressure and soil character and, in certain cases, might prove large enough to make take-off hazardous.

INTRODUCTION

A design requirement of certain aircraft is that they be capable of conducting operations from hastily prepared, unpaved airfields, either on a routine basis or in emergencies. In the past, aircraft intended for this type of operation have been relatively light and slow, but this requirement has recently been expanded to include very heavy and very fast aircraft. Under these conditions, a detailed knowledge of the interaction of a tire with a yielding surface is more critical to the accomplishment of a design which will allow the aircraft to operate safely from substandard fields. Although a great deal of work has been done in the past (refs. 1 and 2, for example) on the problems of operating heavy vehicles in soft soil, little information exists on soil-tire interactions at the high ground speeds associated with aircraft operations. This paper will present some results of a test program in which the towing facilities of the Langley landing-loads track were used to explore the reactions of an aircraft tire operated at high speeds on several different types of soil. Some potential unprepared-field operating problems will also be illustrated. This program was a cooperative venture between NASA, the Air Force Flight Dynamics Laboratory, Lockheed-Georgia Company, IIT Research Institute, and the U.S. Army Engineer Waterways Experiment Station. Although the results

presented in this paper have been reported and compared with analyses in references 3 to 5, the presentation and interpretation of data herein differ. The basic data presented in this paper should serve as a foundation to which future data may be added to establish a tool for further improvement of analytical approaches.

SYMBOLS

Values are given both in the International System of Units (SI) and in the U.S. Customary Units. The measurements and calculations were made in U.S. Customary Units.

F_D	axle drag force
F_{D1}	measured axle drag force, SWDYN, left
F_{D2}	measured axle drag force, SWDYN, right
F_L	axle lateral force (normal to tire plane)
F_S	axle side force (normal to direction of motion)
F_V	axle vertical force
h	axle vertical position
p_t	tire inflation pressure
V_G	forward velocity
z	average rut depth
z_m	measured rut depth
ψ	yaw angle
ω	wheel angular velocity

ABBREVIATIONS

AI	airfield index
CBR	California bearing ratio
D.C.	direct current
FM	frequency modulated
SAXLE	single cantilevered axle
SWDYN	single-wheel dynamometer
TAXLE	tandem cantilevered axle
WES	U.S. Army Engineer Waterways Experiment Station

APPARATUS AND TEST PROCEDURES

Towing Apparatus

The investigation was conducted at the Langley landing-loads track adapted for this program as shown schematically in figure 1. This test facility employs a water-jet catapult developing up to 1800 kN (400 000 lb) thrust to accelerate a test carriage to the desired speed in a distance of about 120 m (400 ft). The carriage then coasts freely on steel rails for a distance of about 370 m (1200 ft) and is stopped at the end of the run by arresting-gear cables. During the coasting period, where the desired tests are usually performed, the velocity decay is very small owing to the large mass, up to 445 kN (100 000 lb), of the test carriage. A section of a concrete-lined water channel which parallels the main test track was used as a soil test bed and was sited as far as possible from the water-jet catapult to minimize any inadvertent wetting of the soil surface. A paved area was provided adjacent to the soil bed so that the test soil could be processed with minimum wastage and contamination with natural soil. A small temporary building near this paved area served as a field soil test laboratory containing large and small drying ovens, scales and balances, an unconfined-compression-test machine, hand tools, etc. Stockpiles for the clay and sand test-bed materials were located a short distance from the test site. A concrete runway was installed in the channel during the later stages of testing, in the approximate location shown in figure 1, to provide some comparative

hard-surface rolling data particularly in the yawed-rolling regime. The smaller of two test carriages available at the facility was used as shown in the figure to support the test tires and fixtures.

A special support system, shown in the photograph of figure 2 and the schematic of figure 3, was constructed to enable the test tire to be towed at high speeds through the soil beds. As shown in figure 3, a ballast basket was attached to the support frame through pivoted parallel arms, and the test tire and load measuring system was attached to this basket. A hydraulic cylinder was provided to raise and lower the ballast basket, as well as to act as a vertical motion damper during most of the test runs since the only other damping in the system was offered by the tire. The position of the parallel-arm linkage could be located as desired laterally on the test bed by loosening and repositioning the lateral adjustment clamps at the front of the support frame and at the hydraulic cylinder at the top of the frame, as shown in figure 3. In one series of tests, a rigid bar was welded to the main carriage structure at the rear of the fixture, as shown, to provide a mount for a soil profile measurement system. During a series of yawed-rolling tests, a steadying roller, guided by a vertical channel, was installed at the rear of the ballast basket to provide additional lateral stiffness.

Test Tire

The tire used throughout this investigation was a $29 \times 11.0-10$, 8-ply-rating, type III aircraft tire having a nominal inflated diameter of 74 cm (29 in.) and a maximum cross-sectional width of 28 cm (11 in.). The tread pattern consisted of five straight, evenly spaced circumferential grooves having a depth of approximately 0.32 cm (1/8 in.). Military Specification gives a tire inflation pressure of 31 N/cm^2 (45 lb/in^2) for the rated tire load of 22 kN (5000 lb). This pressure was used during the test program. Also used were overinflation pressures of 48 N/cm^2 (70 lb/in^2) and 38 N/cm^2 (55 lb/in^2) and an underinflation pressure of 21 N/cm^2 (30 lb/in^2) to give good comparative data. Gross tire-footprint areas were obtained on a hard surface for three significant test inflation pressures at a tire loading of approximately 19 kN (4200 lb) as follows: 381 cm^2 (59.1 in^2) for 48 N/cm^2 (70 lb/in^2), 559 cm^2 (86.6 in^2) for 31 N/cm^2 (45 lb/in^2), and 777 cm^2 (120.4 in^2) for 21 N/cm^2 (30 lb/in^2). In an attempt to provide a "rigid" tire for comparative purposes, one test tire was filled with a polyurethane foam, foamed and expanded inside the tire, which gave a crushing strength on the order of 1380 N/cm^2 (2000 lb/in^2).

Support Fixtures and Instrumentation

Single cantilevered axle.- The test tire was supported by one of the three test fixtures shown schematically in figure 4. The single cantilevered axle, hereinafter referred

to as SAXLE, figure 4(a), was bolted directly to the bottom of the ballast basket after having been carefully alined with the track rail to minimize yawing and rolling moments. Vertical, drag, and axial loads were obtained through four-arm strain-gage bridge circuits on the axle at the location shown. When brakes were applied, brake torque was isolated from the axle and measured by noting the tension in the brake torque rod shown in the figure. Brake line pressure was also monitored through a pressure transducer located near the brake assembly. Wheel angular velocity, used to detect wheel lockup, was measured by a magnetic pickup mounted on the axle and a segmented ring mounted on the wheel. Vertical position of the ballast basket, and thus of the axle, with respect to the support frame, was measured by a slide-wire mounted parallel to the hydraulic positioning cylinder shown in figure 3. Horizontal position of the test carriage was measured by a photocell interrupter system, with triggering provided by narrow white stripes painted at 3.05-m (10-ft) intervals on the blackened track-rail support wall. Carriage velocity at the beginning of the test section was measured by a standard time-interval counter, and this forward velocity was assumed constant over the remainder of the test bed. A pressure transducer located in the lift cylinder to monitor damping, and vertical and drag accelerometers located at the center of the axle completed the instrumentation on this fixture.

Tandem cantilevered axles.- In order to explore the effects of two wheels running in tandem, two instrumented cantilevered axles were mounted on 1-m (40-in.) centers on a beam as shown in figure 4(b). This beam was mounted on a pivot centered under the ballast basket, with stability in pitch being provided by the spring-and-damper mechanism shown. The instrumentation of this tandem-axle test fixture, hereinafter referred to as TAXLE, was quite similar to that described for the single cantilevered axle, SAXLE, except for repositioning the brake torque rods, as shown in the figure, and providing a potentiometer to measure the bogie-beam pitch attitude. An improved angular-velocity measuring system was developed for TAXLE, in which a drive shaft located in the hollow axle was used to transmit rotary motion from a coupling on the wheel hub to an angular accelerometer and an angular-velocity generator mounted on the rear of the axle support beam. Ballast-basket vertical position, test-carriage horizontal position, and carriage forward velocity were measured as described for SAXLE.

Single-wheel dynamometer.- The single-wheel dynamometer, hereinafter referred to as SWDYN, shown in figure 4(c) was used in the last series of tests primarily to determine braking and yawed rolling characteristics of the test tire in clay soil. This fixture, which has been used in many braked rolling investigations (ref. 6, for example) at the Langley landing-loads track, allows vertical, drag, lateral, and brake-torque measurements to be made with a minimum load interaction. The fixture was bolted to the bottom of the ballast basket through a split-ring clamp, allowing the fixture to be

rotated in either direction and locked to provide a fixed yaw angle for yawed rolling studies. As shown in figure 4(c), two load beams in compression measured axle vertical load; two load beams in tension measured axle drag loads; and one load beam in either tension or compression, depending on the sense of the yaw angle, measured lateral or side loads. Brake torque was isolated and measured by the system of tension links shown. Wheel rotation was transmitted by a toothed timing belt to an auxiliary axle, driving an angular accelerometer and an angular-velocity generator. A six-sided cam operating a set of breaker points was also installed on this axle to provide wheel-angular-displacement information. Vertical and horizontal positions, brake and lift cylinder pressures, and vertical and drag axle accelerations were measured as described for the cantilevered axle.

Recording equipment. - Outputs from all measurement systems were processed by appropriate signal conditioning units and recorded on a 14-channel FM magnetic tape recorder carried onboard the test carriage in an enclosed space at the front of the carriage. The enclosed compartment may be seen in the photograph of figure 2, and the interior view of figure 5 shows the signal conditioning units, amplifiers, FM tape recorder, and the multiplex equipment which was used during tests with TAXLE only. Also shown in this figure is an oscillograph used to record accelerations and loads in the primary carriage structure. A time code generator (not shown in fig. 5) was used to provide run identification and a highly accurate continuous time signal to the tape recorder.

Soil Test Beds

Selection of clay. - The channel used as a soil test bed in this investigation was 2.44 m (8 ft) wide. The bed length of approximately 76 m (250 ft) was selected as a length thought to be sufficient to establish steady-state rolling and braking conditions at the higher test velocities and still hold the volume of soil to be processed for each test bed to a reasonable level. The clay soil used as a test-bed material was provided by the U.S. Army Engineer Waterways Experiment Station (WES) from a borrow pit located near Vicksburg, Mississippi, and approximately 610 m³ (800 yd³) of this soil was delivered to the test site at Langley. The selection of this material - a highly plastic, heavy clay (locally called "buckshot") described in detail in reference 2 - was based upon past WES experience, which indicated the clay to be a very stable cohesive test material with changes in water content occurring slowly with time. Thus, once a soil bed had been established with the proper moisture content, reasonably constant conditions could be maintained for the several days necessary to complete a test series. The clay as used in this test program ranged from a moisture content of 35.4 percent and a dry density of 1340 kg/m³ (83.6 lb/ft³) for the softest test beds to a moisture content of 30.1 percent

and a dry density of 1425 kg/m^3 (89 lb/ft^3) for the hardest test bed. A description of the sequence of events involved in the preparation, installation, maintenance, and removal of a typical clay soil test bed will illustrate the considerable effort expended to provide the most uniform test conditions possible.

Preinstallation clay processing. - The quantity of buckshot clay provided by WES was sufficient to construct two complete test beds plus an allowance for wastage. Accordingly, enough material to construct one test bed was hauled from the stockpile to the processing area (fig. 1) and placed in a windrow about 122 m (400 ft) long, 4.6 m (15 ft) wide, and 0.46 m (1.5 ft) deep. The windrow was staked off into 6.1 m (20 ft) sections and the average moisture content of the batch determined by drying and measuring the weight change of samples taken from each section. Previous laboratory work had indicated the approximate moisture content required to obtain the desired soil bed test strength. Water was added to each section of the windrow in metered amounts and more samples taken at intervals until the required overall moisture content was achieved. Before and during the watering process, the large, self-propelled multiple-pass rotary mixer shown in figure 6 was employed continuously in the preinstallation clay processing to break up the large soil clods and to provide a more uniform soil-water mix. The processed soil was then covered with polyethylene to hold evaporation to a minimum.

Installation of clay in test bed. - Before installing the first test bed, a 15-cm-deep (6-in.) layer of clean, coarse gravel was placed in the bottom of the tank to provide drainage under the clay. The processed soil was placed in the tank in 15- to 20-cm-deep (6- to 8-in.) layers or lifts using a large hydraulic excavator. A small motor grader was used in close coordination with the excavator to provide a uniformly thick layer of loose soil which was then compacted by a heavy pneumatic-tire roller making 10 to 12 passes over the bed for each layer of soil. This process, partly illustrated in figure 7, was repeated until the desired soil depth of 0.76 m to 0.91 m (2.5 to 3 ft) was reached. A small, self-propelled, steel-wheel roller and the small grader, working together and using the channel wall as a reference, conducted final finishing operations to provide a reasonably level, smooth test surface. The completed test bed was then kept covered with polyethylene, except during tire tests, to retain surface moisture.

Measurements of test-bed characteristics. - Many different soil test measurements were performed at intervals throughout the program to determine test-bed properties and uniformity. In addition to the moisture-density measurements conducted during bed preparation and continued at intervals during the test-bed life, these included field CBR (California bearing ratio) tests and AI (airfield index) measurements, as described in reference 7, and penetration-resistance and plate-bearing tests with a specially designed test assembly, as described in reference 3. The greatest statistical reliability may be placed on the AI measurements since those were made at 3.05-m (10-ft) intervals down

the intended track of the tire before each test run, whereas the other measurements were made at irregular intervals as opportunity offered. Airfield index numbers were obtained with the airfield cone penetrometer, which is a hand-operated device with a 30° cone having a 1.29-cm^2 (0.2-in^2) base area. (See fig. 8.) The operator forces the penetrometer into the soil at a slow, uniform rate and calls out each 5.08 cm (2 in.) of depth as denoted by scribed lines on the shaft. An observer then reads and records the penetration resistance indicated by the spring scale in the handle of the penetrometer, which is calibrated in terms of one scale division (one AI number) per 44 N (10 lb) of resisting force. A typical penetration test is shown in progress in the photograph of figure 9. In this program, penetration readings were obtained every 5.08 cm (2 in.) up to a depth of 45.7 cm (18 in.) or a penetration resistance of 660 N (150 lb), whichever occurred first. Although this paper will use only airfield index measurements in discussion of data because of the greater sampling frequency, figure 10 shows the approximate correlation of AI with CBR for the clay used in this program.

At the same location and 3.05-m (10-ft) interval as the AI measurements, elevations of the soil-test-bed surface with respect to the track rail were obtained before each test run by using a standard rod-and-level survey technique. The survey was repeated after the test run to enable some determination to be made of the amount of soil deformation, or rutting, caused by the tire for each test condition. These measurements proved of such potential importance that the profilometer shown in figure 11 was developed and used during the later phases of the program to provide a continuous measure of test-bed elevation with respect to the test carriage.

Maintenance of clay test bed. - Test-bed maintenance was concerned primarily with repairing surface damage caused by the test tire during a run. At the higher soil strengths and higher test speeds, bed damage was minimal and, by translating the test fixture laterally, as many as four runs could be made before any surface repair was necessary. At the lower soil strengths and lower speeds, however, extensive surface repair became necessary, sometimes after every test run. Fortunately, in the range of moisture content used in these tests, field measurements showed the strength of the buckshot clay to be nearly independent of the effort of compaction. Thus, many of the shallow ruts could simply be rolled flat with the steel-wheel roller, and the surface could then be releveled with the grader. Deep ruts caused by heavy braking at low speeds required use of the pneumatic-tire roller to make a sufficient number of passes to reduce the ruts to a depth which could be leveled by the steel-wheel roller. Occasionally, also, evaporation of water from the test-bed surface caused the formation of a thin, hard crust which had to be cut from the bed with the grader. The new surface was then lightly wetted and rolled with the steel-wheel roller to make it ready for testing.

Between testing and test-bed maintenance operations, more soil was transferred from the stockpile to the processing area, and moisture conditioning was initiated to prepare for the next desired soil strength.

Preparation of sand test bed. - Installation of the sand test bed followed the same general procedures outlined for installation of the buckshot clay. The sand material used for these tests was obtained locally and was a poorly graded, medium sand of river origin. Only one sand test bed was constructed, and, as finally graded and compacted, the sand had a density of approximately 1666 kg/m^3 (104 lb/ft^3) and a moisture content of 6 to 8 percent. A good deal of difficulty was encountered in emplacing this bed, but a bed having essentially constant density was achieved and maintained for this test series. Soil test measurements also followed the general procedure outlined for the clay tests, with airfield index and elevation measurements being taken at 3.05-m (10-ft) intervals down the intended tire path before each test run. At these same locations, samples of the sand were taken to establish surface density and water content.

Sand-test-bed maintenance involved grading and compacting the bed to remove ruts caused by the tire tests. Because of the large amount of sand displaced by the wheel, only two test lanes were used in sand with the lanes located 0.305 m (1 ft) on each side of the center of the bed. When a level surface had been achieved, the surface was sprinkled lightly with water to replace lost surface moisture and was then covered with polyethylene until the test.

Tire Test Procedure

The same general tire test procedures were followed on both clay and sand test beds. On each new bed of different soil character and for each change in tire inflation pressure, a series of preliminary tests were run prior to the catapult tests. The first test conducted was a static sinkage test in which the tire was lowered to the soil surface and allowed to sink under full ballast load until steady-state conditions were reached. The tire was then raised clear of the soil and the carriage was moved forward a few meters. In the second test, the tire was allowed to sink again into the soil and the carriage was towed forward a few meters with the tire in the soil to establish a quasi-drawbar-pull drag value. In the final test, the tire was raised clear of the soil and the carriage was towed back a sufficient distance to allow the towing tractor to accelerate the carriage to 6 to 8 knots for a low-speed test. When a constant forward speed was reached, the tire was lowered into the soil and, after steady-state free-rolling conditions were established, the brakes were locked for a short distance to establish braking drag values. The brakes were then released and the tire raised clear of the bed. All these tests were accomplished in one lane or track near the downstream end of the soil bed,

most often leaving enough virgin soil at the upstream end to permit a low-speed catapult run.

Before any catapult run was made, the test fixture was positioned as desired laterally, then raised to its maximum height and locked. Tire and brake pressures were set and all data channels balanced and checked at the recorder. Knife edges were placed on the track according to the desired speed of each run in order to actuate switches to drop the tire at the desired location and to apply brakes at the proper time. A restriction in the discharge line of the hydraulic lift cylinder reduced the vertical impact velocity at ground contact and also acted as a vertical-motion damper during the run.

DATA-REDUCTION PROCEDURES

Averaging Techniques for Airfield Index

The summarizing and comparative data to be presented in a subsequent section of this paper have of necessity been subjected to a great deal of averaging of both soil-test-bed conditions and resulting axle loads. Although each soil bed was constructed and maintained as carefully as possible, the field test environment did cause a certain degree of nonuniform soil conditions. Table I shows how airfield index readings obtained with the airfield cone penetrometer varied with depth and location along a typical clay test bed. The gradual increase in penetration resistance with increasing depth was typical for all clay test beds and was thought to be partly due to penetrometer-shaft drag caused by insufficient relief between cone and shaft (fig. 8). In spite of this high-side bias, airfield index (AI) will be the standard used in this paper to compare one soil condition with another, since these measurements were made in the intended track of the tire before each run and should give the best picture of changing test conditions. Since tire penetration in clay seldom exceeded 15.2 cm (6 in.) and in order to minimize shaft-drag bias, AI values were averaged for the 0- to 15.2-cm-depth (0- to 6-in.) measurements at each test-bed station, as noted in table I. The values were averaged to give an AI number for that particular run (AI = 1.4 for the run shown). The AI numbers for each run were then averaged to determine an overall average AI for each test series or test bed.

Averaging Techniques for Rut Depth

A further variation was introduced by test-bed surface unevenness such as shown in figure 12(a), which is the test-bed profile before the run as measured by the profilometer pictured in figure 11. The exact effect of surface unevenness is unknown, since at this time it is impossible to measure or isolate the interplay of tire deflection, tire distortion, and soil springback. That a good deal of smoothing took place during the run

can be inferred by comparing figure 12(a) with figure 12(b), the before-run and after-run profiles, but how this smoothing or rolling action affected the measured axle drag load is not known. Rut depth in this paper is defined as the difference between elevation measurements made at the same soil-bed location before and after each test run, and is shown in figure 12(c) as obtained from both the continuous-reading profilometer and the rod-and-level survey technique described earlier. The rut-depth profile z_m developed by either method was then averaged over the same interval as the measured axle loads to obtain the average rut depth z to be presented in a subsequent section. For illustration, the average airfield index obtained from table I for this test bed is included in figure 12(a).

Averaging Techniques for Axle Loads

The final averaging process was concerned with the measured axle loads during each series of tests. Typical time histories of vertical load, drag load, wheel angular velocity, and axle vertical position are shown in figure 13 for the same test run for which the soil test conditions were shown in figure 12. The extreme variations in measured loads are obvious and are thought to be due in part to the uneven soil surface and the nonuniform soil strength discussed previously and in part to noise induced by the basic carriage structure and poor system damping. In either case, in order to permit meaningful load comparisons between various test parameters, load averages were made over that period in each test run where near-steady-state conditions seemed most likely to occur, due regard being given to all sources of information about that run. Vertical- and drag-load averages were obtained during free rolling on concrete, free rolling on clay or sand, and locked-wheel braking in clay or sand, for all test runs where these conditions occurred. No attempt was made to obtain load averages in the transient zones indicated in figure 12, or for braking conditions other than locked-wheel braking. In the comparisons made in the rest of this paper, the average drag loads have been normalized by dividing by the average vertical loads, and in each case the ratio is expressed as axle drag coefficient (F_D/F_V).

RESULTS AND DISCUSSION

General Considerations

In the course of this investigation of aircraft tire behavior during high-speed operations in soil, a great many variables were examined in more or less detail. In all these tests, forward velocity was considered as the prime independent variable. A set of six or eight discrete, preselected velocities constituted a test series for investigating the effect of other parameters on the prime dependent variables of axle drag load

and rut depth. These parameters included four different tire inflation pressures, four clay test beds of different strength characteristics, one sand bed, and one concrete surface. Limited braking and yawed rolling studies were also made at some of the test conditions. The effects of these various parameters and test conditions will be discussed in the following sections.

Free-Rolling Axle Drag Coefficients

Single-wheel dynamometer tests.- As mentioned previously, all testing was done with the three fixtures shown in figure 4. Of these fixtures, the single-wheel dynamometer (SWDYN) has been used for several years in various braking and cornering investigations (see ref. 6, for example) at the Langley landing-loads track, and a good deal of experience and confidence has been gained in this load-measuring system. Also, the SWDYN series was among the last, chronologically, to be run in this investigation and benefited thereby from the experience in soil handling and testing techniques gained during the earlier series. For these reasons and because the most complete soil-test-bed information was obtained for these tests, the SWDYN series is considered to have provided the best quality data of the program. These data increased confidence in the earlier results obtained with the single cantilevered axle, which constituted the bulk of the data, since the same data trends were observed in both series. Figure 14 shows the axle drag coefficients and resulting rut depths developed by the SWDYN operating at a 48-N/cm^2 (70-lb/in^2) tire pressure on AI 1.5 clay compared with the results for the same free-rolling conditions on concrete. The large increase in drag coefficient due to operation in clay is immediately obvious, in some cases being nearly 10 times the equivalent drag coefficient or rolling resistance experienced on concrete. It will be noted that this hard-surface rolling resistance is somewhat higher than might be expected and may be a characteristic of the low-pressure, type III test tire. Results to be presented subsequently will confirm that the shape of the drag-coefficient curve in soil is characteristic for nearly all test conditions, with the drag loads initially decreasing from static or low speed and then rising sharply with increasing forward speed to a peak in the velocity range of 40 knots. The change in drag coefficient is reflected to a certain degree by changes in the average rut depth as shown in figure 14. The phenomena causing the changing drag load with velocity are not clearly understood, but are thought to be related to changes in soil mechanical properties with increased effective loading rate and possibly to some change in tire shape producing changes in immersed body lift and drag coefficients.

Effects of changing clay strength.- The effects of changing clay strengths on the axle drag coefficients and rut depths developed by SAXLE are shown in figures 15(a) and 15(b), respectively, for a tire inflation pressure of 48 N/cm^2 (70 lb/in^2). An overall

decrease in drag coefficient with increasing soil strength is shown, with the stronger soil trending toward the rolling-resistance values developed on concrete. No rut-depth measurements were obtained for the AI 3.2 clay because penetration into the soil was insignificant. This fact further suggests that, for this tire and load combination, no operational problems would be expected on clay soil stronger than AI 3.2.

Effects of vertical load.- The effects of reduced vertical load are shown in figure 16, where the SAXLE nominal vertical load of 23.1 kN (5200 lb) was reduced to 11.6 kN (2600 lb) for one test series. This load reduction significantly reduces the peak or hump in the axle-drag-coefficient curve but has little apparent effect in the low- and high-speed regimes. However, a significant reduction in rut depth is noted for the lighter load at all speeds.

Effects of tire inflation pressure.- The preceding results suggest that drag coefficients may not be directly related to rut depths, but may depend on other parameters. One parameter may very well be tire inflation pressure, as illustrated in figure 17 where axle drag coefficients and rut depths are shown as a function of forward velocity for four tire inflation pressures. The tire pressures were chosen to represent a realistic operating range for this tire, as explained previously. Figure 17(a) shows the strong dependence of axle drag coefficient upon tire inflation pressure, where reducing pressure from 48 N/cm² to 21 N/cm² (70 lb/in² to 30 lb/in²) is seen to reduce peak axle drag coefficients by more than one-half. The same trend in rut depth is noted in figure 17(b), but the reduction in rut depth is nearly two-thirds and persists over the entire velocity range. From figure 17(a), it also appears that reducing tire inflation pressure does not appreciably change the speed at which the peak drag load occurs. A similar drag-load peak occurs for a tire operating on a water- or slush-covered runway owing to the onset of hydroplaning (ref. 6), but lower tire pressures produce much lower hydroplaning speeds. This point suggests, then, that the peak in the soil-drag-coefficient curve is related more to soil properties than to tire properties. Furthermore, examination of the drag-load curve for a 21-N/cm² (30-lb/in²) inflation pressure reveals a slight increase at the highest test velocities, a fact confirmed by two different tests conducted a week apart. Equipment speed limitations, however, prevented further exploration of this phenomena.

Although the data of figure 17 were for clay of AI 1.6, the same dependency of axle drag coefficient on tire inflation pressures occurs in stronger soil as shown in figure 18 for AI 2.0 clay. A definite peak in the drag-load curve is observed in figure 18(a) for the 48-N/cm² (70-lb/in²) and 31-N/cm² (45-lb/in²) tire pressures, with all drag coefficients notably reduced in magnitude with reductions in tire inflation pressure. For the 21-N/cm² (30-lb/in²) tire pressure, no clearly defined peak appears, possibly owing to scatter or inaccuracy of the data as drag loads approach the level of those measured on concrete. The rut depths developed by SAXLE in AI 2.0 clay are seen to follow the same

general trends noted in AI 1.6 clay for all three tire inflation pressures, although the degree of penetration is much less. (See fig. 18(b).)

As mentioned previously, some tests were run with a so-called rigid tire filled with polyurethane foam in an attempt to isolate the effects of tire deformation from the effects of soil deformation. Unfortunately, tire bounce due to insufficient system damping casts doubt on the measured load data, but it is significant to note that the soil failure mode during free rolling resembled that occurring during locked-wheel braking with a pneumatic tire.

Comparison of clay and sand data.- Up to this point, all tests discussed have been those in which buckshot clay was used in the soil test bed. This type of clay is an almost purely cohesive soil whose strength or resistance to penetration is determined by cohesive bonds between soil particles. However, the strength of most in situ soils depends upon some combination of cohesion and internal friction, that is, the resistance to penetration caused by friction of individual soil particles at their contact point. Quite different penetration resistance characteristics occur in sand and in clay as shown in figure 19 where the average airfield index reading with depth for the sand test bed is compared with the readings for a typical clay test bed. The sudden reduction in penetration resistance of the sand at the 30.5-cm (12-in.) depth is thought to be due to poor drainage of the test bed. Test holes dug in the sand at intervals along the bed revealed that capillary action of water from the channel floor had created a false water table in the sand, with standing water observed in the holes at a level of about 0.76 m (2.5 ft) above the channel floor. It is uncertain how this phenomenon affected the test results, although tire penetrations seldom exceeded 5 cm (2 in.) except during braking.

Axle drag coefficients and rut depths for the SAXLE tests in sand at tire inflation pressures of 48, 31, and 21 N/cm² (70, 45, and 30 lb/in²) are shown in figure 20(a) and figure 20(b), respectively. The variation in drag load with forward speed in sand is similar to that found in clay, as compared in figure 20(a), although the magnitude of the load is smaller. The results shown suggest that operations in natural soil, having combined cohesive and frictional properties, will reflect a hump or peak in the drag-load curve which may rise to a significant level. Drag coefficients of this magnitude may prove helpful in stopping an aircraft, but could greatly increase the required take-off distance.

Other Ground Operating Problems

Braking drag coefficients.- The braking problem was investigated in a limited way, with brakes being applied for a short distance following steady-state free rolling. The most complete braking data were obtained during tests of the SWDYN. As shown in figure 21(a), locked-wheel axle drag coefficients greatly exceed the free-rolling values at

all speeds, but do show the same tendency to reach a peak value near 40 knots. As noted for the free-rolling cases, the rut depths shown in figure 21(b) do not necessarily follow the same trends as the drag coefficients, although rut depths for braking are generally higher than those for free rolling except at the highest speeds. For this series only, rut cross sections were obtained by driving an aluminum plate into the soil across the ruts left by the tire during free rolling and braking. Paint was then sprayed over these plates to leave a silhouette of the rut cross section. Tracings of these silhouettes are shown in figure 22 for the free-rolling and locked-wheel braking series presented in figure 21. A profile of the inflated but unloaded tire is included for comparison. It can be noted from these profiles that measuring rut depths from the reference elevation shown does not give a true picture of the soil actually displaced by the tire. For instance, in figure 22(b), the measured rut depth during braking is approximately 8.9 cm (3.5 in.) whereas the distance from the lowest point to the highest point is approximately 17.8 cm (7.0 in.).

The difference in the method of soil failure during free-rolling and braking is shown in figure 23. The free-rolling rut was characteristically smooth and offered a clean, well-molded contour clearly showing the tire tread pattern. This pattern could be observed also in the braking rut, but the soil clearly failed in shear, with a great amount of material being displaced outside the rut. In fact, some of this material was dispersed so widely as to suggest a possible operating problem should chunks of soil impinge on the aircraft structure during braking. Movies taken during these runs also showed a great deal of material being ejected ahead of the locked wheel, and this inferred the presence of a bow wave of some magnitude in the soil. An indication of the size of this bow wave is shown in the photograph of figure 24. This photograph was taken after a sink-and-tow or drawbar-pull test, described earlier, when the carriage had stopped and the tire was raised vertically. A static sinkage footprint may be observed in the background.

Rut appearances similar to those for clay were noted during braking and free rolling in sand, as shown in figure 25 where the free rolling rut is in the foreground, locked-wheel braking in the middle distance, and free rolling again in the background. Note the heavy amount of sand displaced on and over the top of the channel during braking, an indication of a different type of soil failure than during free rolling. It should be remarked in passing that this type of failure took place in sand whenever any significant brake torque was applied to the wheel, as contrasted with the shearing failure in clay which took place only when the wheel was locked.

As mentioned previously, some braking was attempted during the latter part of most of the free-rolling runs, but in the early runs wheel lockup was not possible at speeds much above 40 knots. The reason for this is not understood although the opposite trend would normally be expected on concrete. However, the brake used in the early SAXLE series was replaced with a larger one for the SWDYN series, and lockup then

occurred for all test speeds. Comparison of braking values in soils for conditions other than full skid, or locked wheel, will not be attempted in this paper owing to a lack of definition of effective rolling radius, and hence of tire slip ratio, when the surface is penetrated. The change in rolling radius may be significant, as shown by the wheel-angular-velocity trace of figure 13 where an abrupt change is noted as the tire goes from concrete to clay. However, this abruptness may also be due to the presence of tire slippage even under free-rolling conditions in clay, a fact which could cause improper antiskid system operation under these conditions. The locked-wheel axle drag coefficients obtained for those few conditions where wheel lockup was achieved are presented in figure 26 for AI 1.6 clay and for sand. The drag coefficients are seen to be very high, just as observed for SWDYN in figure 21, and increased somewhat with velocity up to 40 knots. If the trends established in figure 21 are valid for all cases, these values are probably near maximum and will likely diminish with increased velocity.

A potential operating problem not investigated at all is suggested by the photograph of figure 27, showing the touchdown and wheel spin-up area during a typical run in clay. The sink rate used in these tests was very low, of the order of a few centimeters per second, because there was no shock strut in the system. However, the photograph shows the same type of soil failure experienced during locked-wheel braking, and it might be expected that very high spin-up drag loads might be encountered at the high sink rates common among assault airplanes.

Side-force coefficients.- Limited studies were made to compare the yawed rolling (cornering mode) characteristics of a tire on concrete and on soil with the SWDYN at yaw angles of 3° and 6° . The tests encompassed a full velocity range; however, they were made for one tire inflation pressure and one soil strength only. Side force is defined herein as the force developed normal to the direction of motion, and drag force, as the force in opposition to the direction of motion. These forces were derived (see fig. 28) from the loads measured by the beams shown in figure 4(c). The results of the yawed-rolling studies are summarized in figure 29, where side-force coefficients at yaw angles of 3° and 6° are compared for concrete and for clay. The drastic reduction in side force which is seen to occur when going from concrete to clay is a clear indication of a potential loss of ground maneuverability for aircraft operating from unprepared fields. Yaw angle is shown to have only a slight effect on drag force coefficient and no significant effect on rut depth as shown in figure 30(a) and figure 30(b), respectively.

As illustrated in figure 31, should locked-wheel braking occur when the tire is yawed, the already meager side forces drop to insignificant values. This effect, which is similar to the combination of braking and loss of steering noted for tires operating on concrete in reference 8, adds further emphasis to the need for cautious brake application when operating in soil. The braking drag forces are not greatly influenced by yaw angle,

as shown in figure 32, although a moderate increase over the 0° yaw case is noted here, as well as for the unbraked condition shown in figure 30.

Effect of tandem wheels.- In order to determine the gross effects of two wheels operating in tandem, a brief test series was conducted using the tandem-axle test fixture (TAXLE) shown in figure 4(b). This fixture was run only on the clay soil test bed having an average airfield index of 1.5. Unfortunately, test-carriage structural limitations prevented ballast loading of the TAXLE fixture to the equivalent single-wheel loading used in the SAXLE series; therefore, additional vertical loading was attempted by using the hydraulic positioning cylinder shown in figure 3. After a short test series, it was found that loads of this magnitude were dangerously stressing the test-carriage structure; therefore, the heavyweight series was discontinued and the rest of the TAXLE investigation was conducted at the lighter load. Although incomplete, the results of the heavyweight series are presented in figure 33, with axle drag coefficients for each axle compared with the results for a similar SAXLE series conducted on clay of AI 1.6. The drag coefficients for the tandem wheels are of the same order of magnitude as a single wheel but apparently have a different relationship with forward velocity. At the heavyweight condition ($F_V \approx 22$ kN or 5000 lb per wheel), there is an obvious difference in the drag loads experienced by the leading wheel and the trailing wheel with, surprisingly, the trailing wheel experiencing the higher drag load. No such clear-cut distinction is noted in the lightweight cases ($F_V \approx 11$ kN or 2500 lb per wheel) shown in figure 34, although considerable variation in drag load exists between leading and trailing wheels. Some of the same trends are noted for the tandem wheels as for the single wheels, particularly the higher tire pressures resulting in higher drag loads and an apparent hump or peak in the drag-load curve near a forward speed of 40 knots. The rut depths measured for these test conditions are shown in figure 35 and, again, are compared to similar SAXLE test series on AI 1.6 clay.

CONCLUSIONS

An investigation to determine the relationships between tire and ground when operating in soils at high speeds has been made and some of the problems which might be encountered should such operations become necessary have been explored. Significant conclusions of this program are summarized as follows:

1. In general, axle drag loads are highly dependent on forward velocity, with loads initially decreasing from static or low speed and then rising sharply with increasing forward speed to a peak in the velocity range of 40 knots for the configurations tested. Further increases in speed bring about a reduction in drag load by phenomena not presently understood.

2. In a given soil strength, the magnitude of the axle drag loads is strongly a function of tire inflation pressure, with higher inflation pressures resulting in higher axle drag coefficients.

3. Changing soil strengths or soil character altered the magnitude of the peak in the drag-load curve, although the peak was still present in most cases. In certain soil strength and tire pressure combinations, the axle drag coefficients rose to a level sufficient to be troublesome at take-off for some aircraft.

4. Braking in soft soils will cause operating problems because of the high drag loads and because of the large amount of soil displaced from the locked wheel with consequent possible impingement on aircraft surfaces. Furthermore, proper antiskid system operation is questionable in these circumstances since a change in effective rolling radius occurs with soil penetration.

5. Problems may be encountered in developing enough side forces for adequate ground maneuverability on soft soils. As on concrete, complete loss in steering forces will occur should the wheels become locked.

6. The load relationship between wheels in a tandem pair is quite complex. The brief test program described in this paper indicated no significant difference in the magnitude of drag load or rut depth for tandem wheels when compared with the results for a nearly equivalent single-wheel axle; however, in some cases, the trailing wheel experienced a higher drag load than the leading wheel.

Langley Research Center,
National Aeronautics and Space Administration,
Hampton, Va., June 30, 1972.

REFERENCES

1. Wismer, R. D.: Performance of Soils Under Tire Loads. Rep. 3 - Tests in Clay Through November 1962. Tech. Rep. No. 3-666, U.S. Army Eng. Waterways Exp. Sta., Corps Eng., Feb. 1966.
2. Smith, J. L.: Strength-Moisture-Density Relations of Fine-Grained Soils in Vehicle Mobility Research. Tech. Rep. No. 3-639, U.S. Army Eng. Waterways Exp. Sta., Corps Eng., Jan. 1964.
3. Crenshaw, B. M.; Butterworth, C. K.; and Truesdale, W. B.: Aircraft Landing Gear Dynamic Loads From Operation on Clay and Sandy Soil. AFFDL-TR-69-51, U.S. Air Force, Feb. 1971.
4. Crenshaw, B. M.; Truesdale, W. B.; and Nelson, R. D.: Aircraft Landing Gear Dynamic Loads Induced by Soil Landing Fields. AFFDL-TR-70-169, vols. I and II, U.S. Air Force, June 1972.
5. Crenshaw, B. M.: Soil/Wheel Interaction at High Speed. [Preprint] 710181, Soc. Automot. Eng., Jan. 1971.
6. Horne, Walter B.; and Leland, Trafford J. W.: Influence of Tire Tread Pattern and Runway Surface Condition on Braking Friction and Rolling Resistance of a Modern Aircraft Tire. NASA TN D-1376, 1962.
7. Anon.: Materials Testing. TM 5-530 and AMF 88-51, U.S. Army and U.S. Air Force, Feb. 1966.
8. Byrdsong, Thomas A.: Investigation of the Effect of Wheel Braking on Side-Force Capability of a Pneumatic Tire. NASA TN D-4602, 1968.

TABLE I.- MEASURED AIRFIELD INDEX (AI) VALUES AND AVERAGES OBTAINED FOR A TYPICAL CLAY TEST BED

*Test-bed station		AI readings at depths shown:										Average AI for 0 to 15.2 cm (0 to 6 in.) of depth
		0 cm	5.1 cm	10.2 cm	15.2 cm	20.3 cm	25.4 cm	30.5 cm	35.6 cm	40.7 cm	45.7 cm	
m	ft	0 in.	2 in.	4 in.	6 in.	8 in.	10 in.	12 in.	14 in.	16 in.	18 in.	
24.4	80	2	1.5	1.5	2	2	2	2.5	3	3	3	1.75
27.4	90	1.5	1	1.5	2	3	3	4	4.5	5	5	1.5
30.5	100	1.5	1	1	1.5	1.5	1.5	2	1.5	1.5	2	1.25
33.5	110	1	1	1.5	1.5	2	2	2	2	2	2.5	1.25
36.6	120	1	1	1.5	1.5	1.5	1.5	1.5	2	2	3	1.25
39.6	130	2	1	1.5	1.5	1.5	2	2	2	2	2	1.5
42.7	140	1.5	1	1	1.5	2	2	2	2.5	2.5	2	1.25
45.7	150	1	1	1.5	1.5	1.5	2	3	3.5	4	5	1.25
48.8	160	1.5	1	1	1	1	1.5	1.5	1.5	2	2.5	1.13
51.8	170	2	1.5	1	2	2.5	2.5	3	3	3	2.5	1.63
54.9	180	1	1	1	1.5	1.5	2	2.5	3	3.5	4	1.13
57.9	190	1.5	1	1	2	2	2.5	3	4	4	4.5	1.38
61.0	200	1.5	1.5	1	1.5	2	2.5	3	3.5	4	5	1.38
64.0	210	---	---	---	---	---	---	---	---	---	---	----
67.0	220	2	1.5	1.5	2	2	2.5	2.5	3.5	4.5	5	1.75
70.1	230	1.5	1	1	1.5	2	2	2	2	2	2.5	1.25
73.1	240	1	1	1	1.5	1.5	1.5	2	2	3	3.5	1.13
76.2	250	1.5	1	1.5	1.5	2	2.5	3.5	3.5	4	5	1.38
79.3	260	1	1	1.5	1.5	2.5	3	3.5	4	5.5	5.5	1.25
82.3	270	1	1	1.5	1.5	2.5	2.5	3	4.5	4.5	5	1.25
85.3	280	1	1	1.5	1.5	1.5	1.5	2	2.5	3	3.5	1.25
88.4	290	1	1.5	1.5	1.5	3	3.5	3.5	2	2.5	2.5	1.38
91.4	300	1	1.5	1.5	1.5	1.5	2	2	2	2	2.5	1.38
94.5	310	1	1.5	1	1.5	1.5	2	2	2	2.5	2.5	1.25
97.5	320	1	1	1.5	2	2.5	3.5	4	4.5	4.5	5.5	1.38
100.6	330	1	1.5	1	2	3	3.5	3.5	5	5.5	6	1.38
103.6	340	1	1.5	1.5	2.5	2.5	3	3.5	3.5	4.5	5	1.63
106.7	350	1	1.5	1.5	2	1.5	1.5	1.5	2	2	1.5	1.5

Test bed average = 1.4

*Stations measured at 3.05-m (10-ft) intervals.

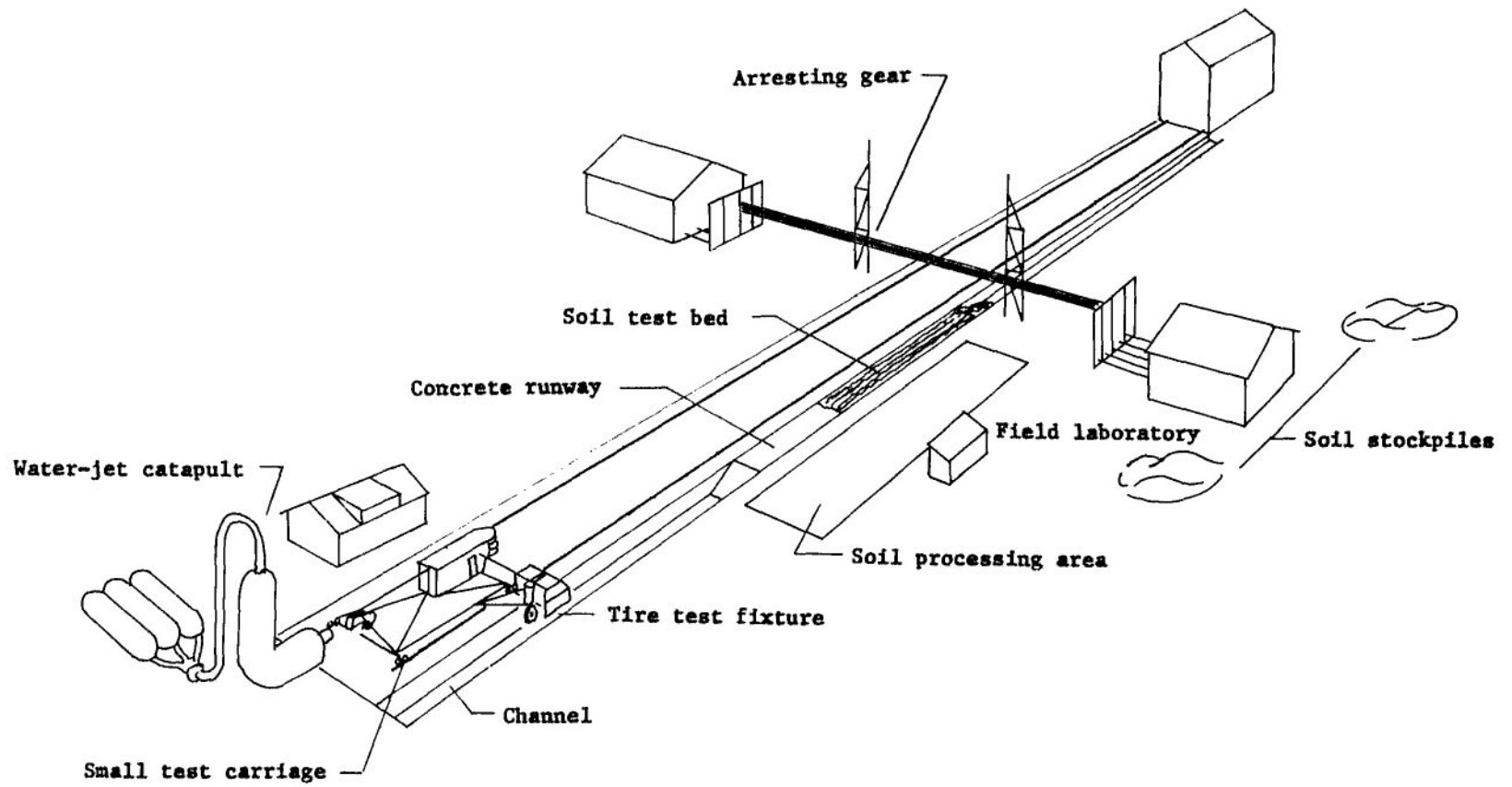
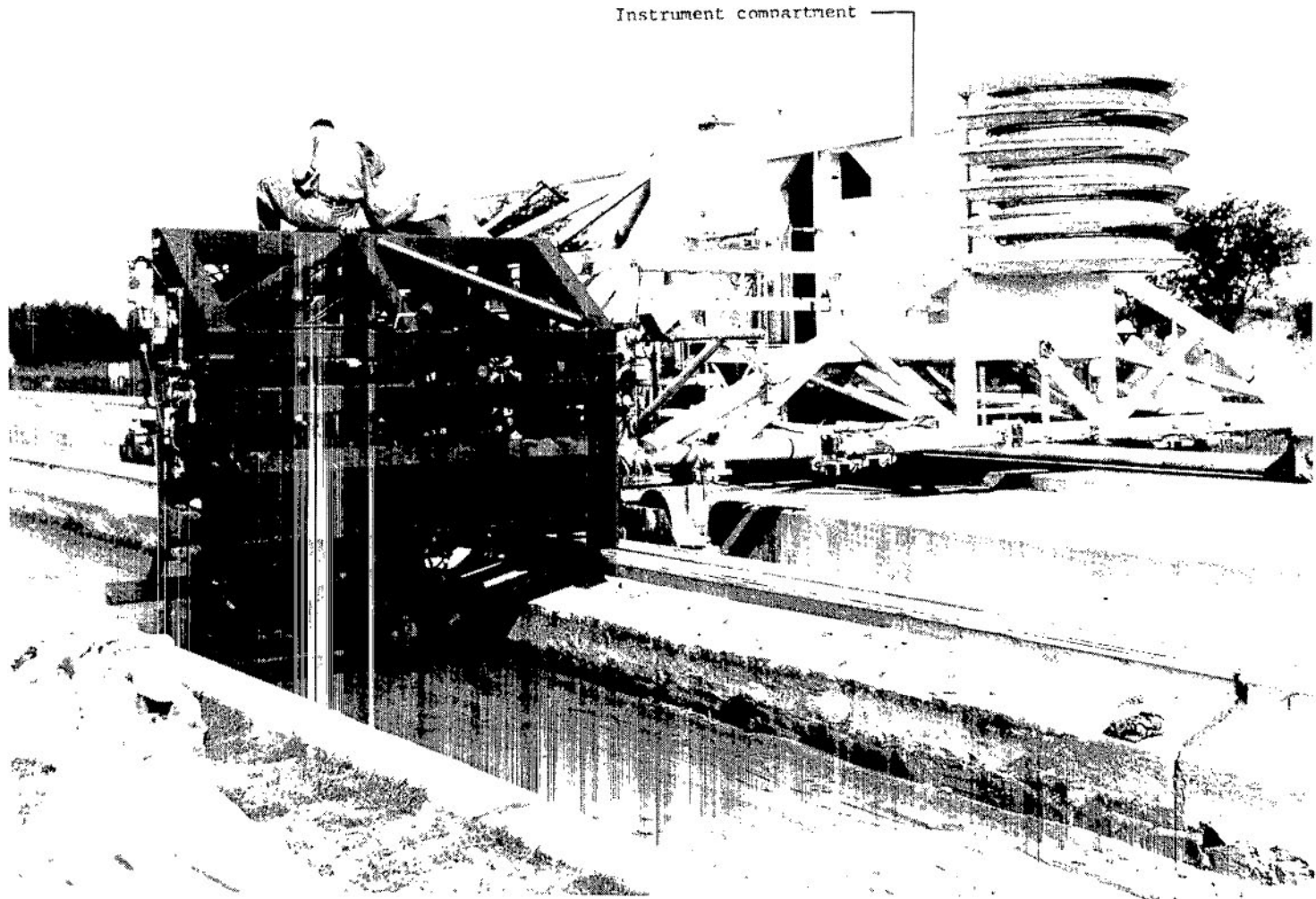


Figure 1.- Schematic of Langley landing-load track as arranged for soils test program.



L-69-5535.1

Figure 2.- Small test carriage with tire test fixture installed.

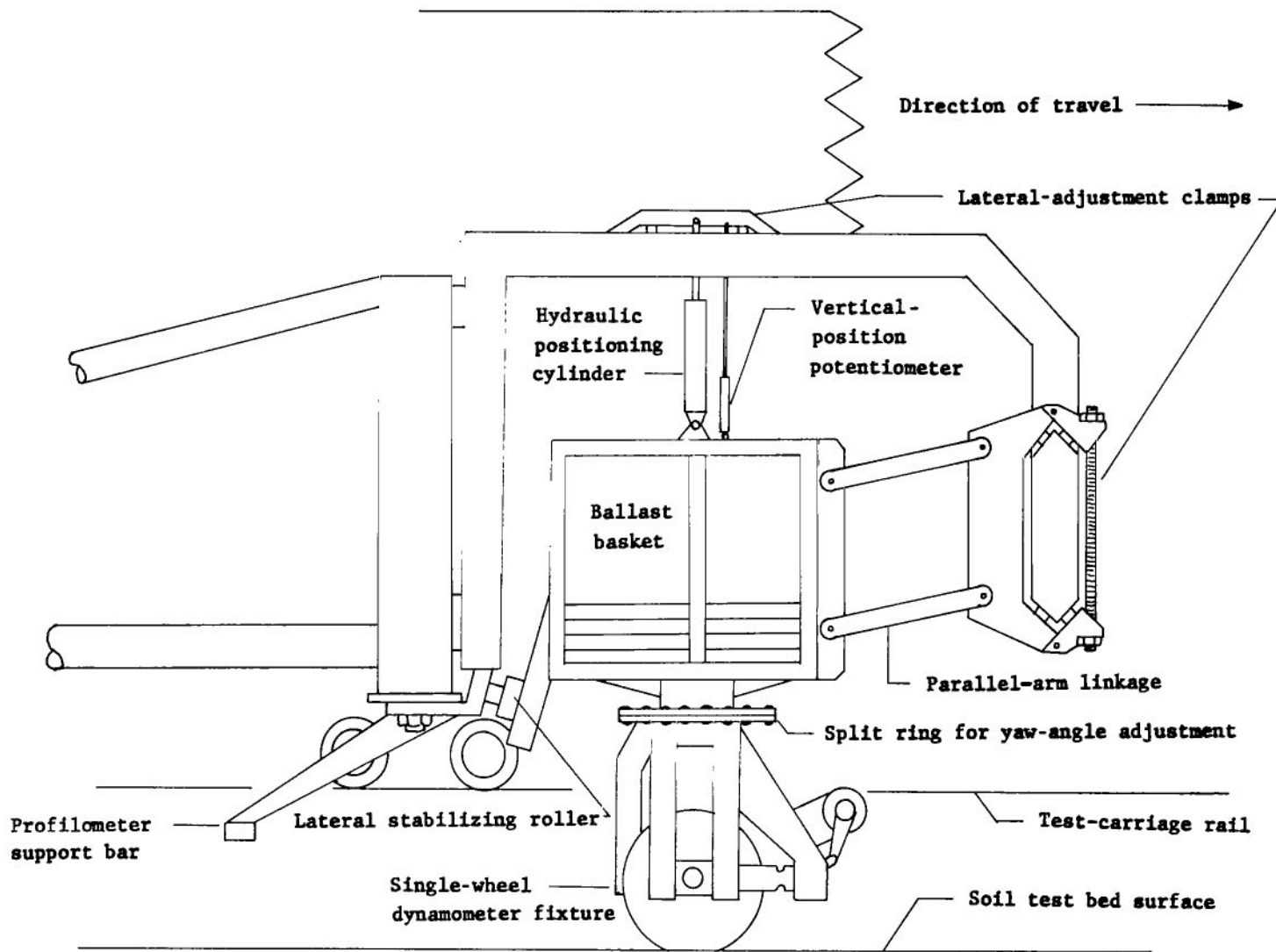


Figure 3.- Schematic of tire test fixture support structure.

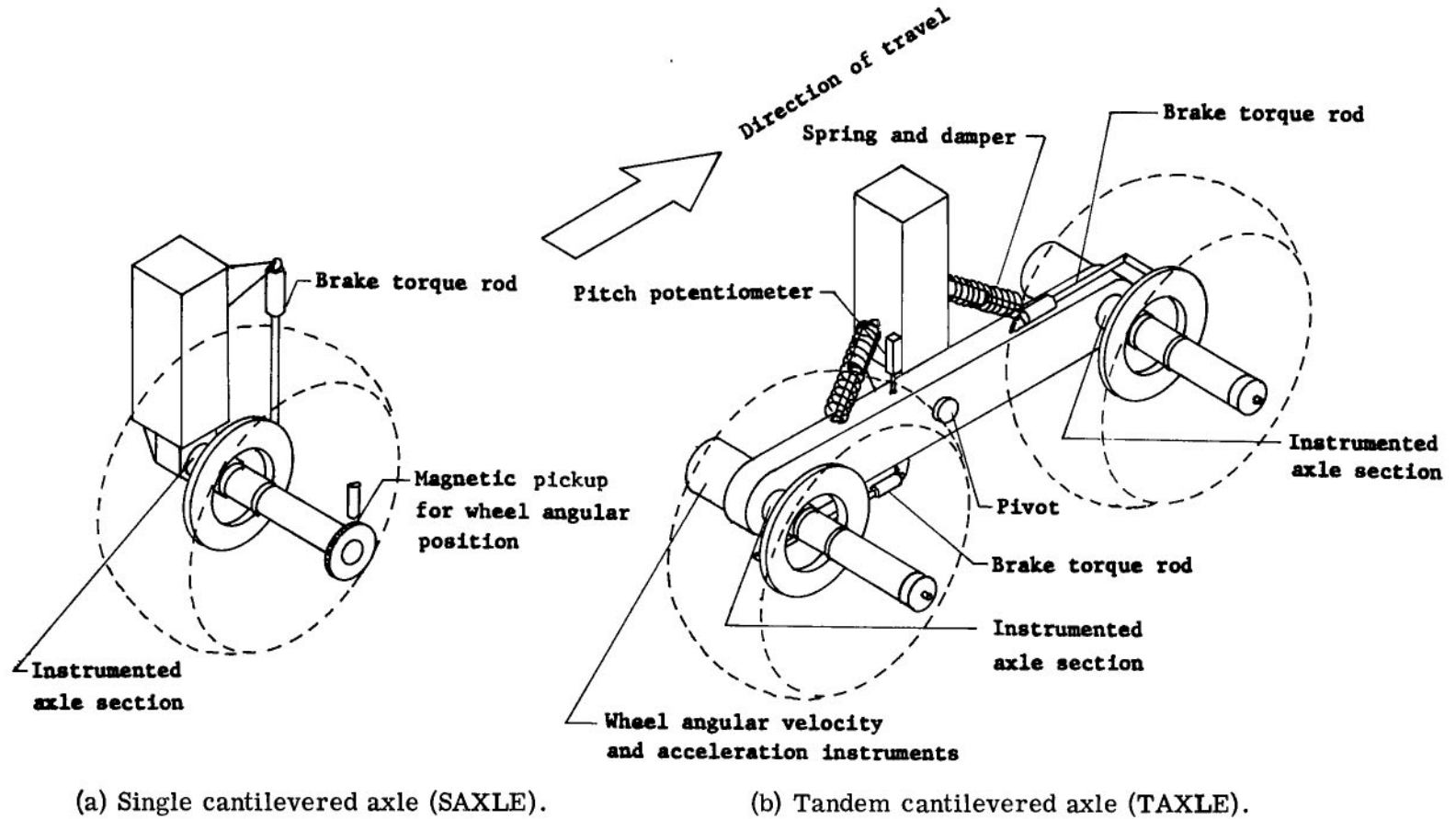
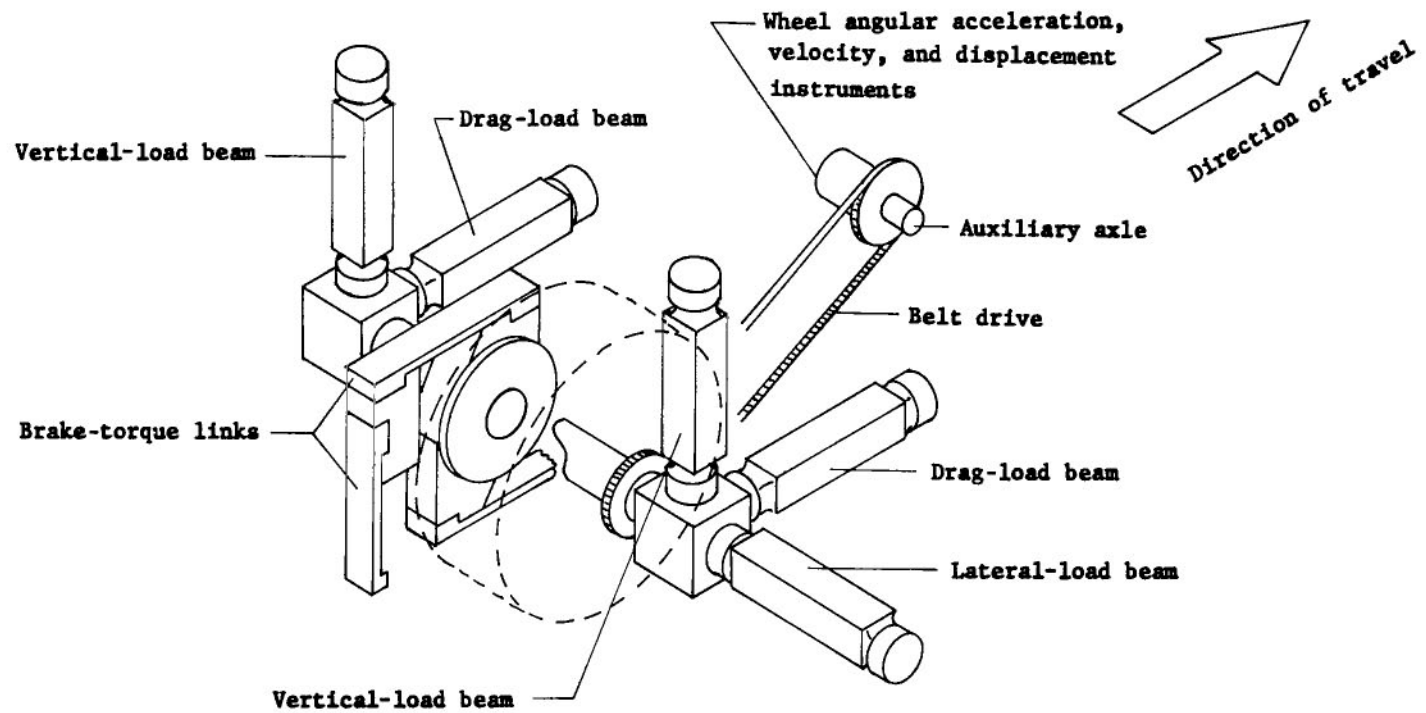


Figure 4.- Schematic of test fixtures used in the soils test program.



(c) Single-wheel dynamometer (SWDYN).

Figure 4.- Concluded.

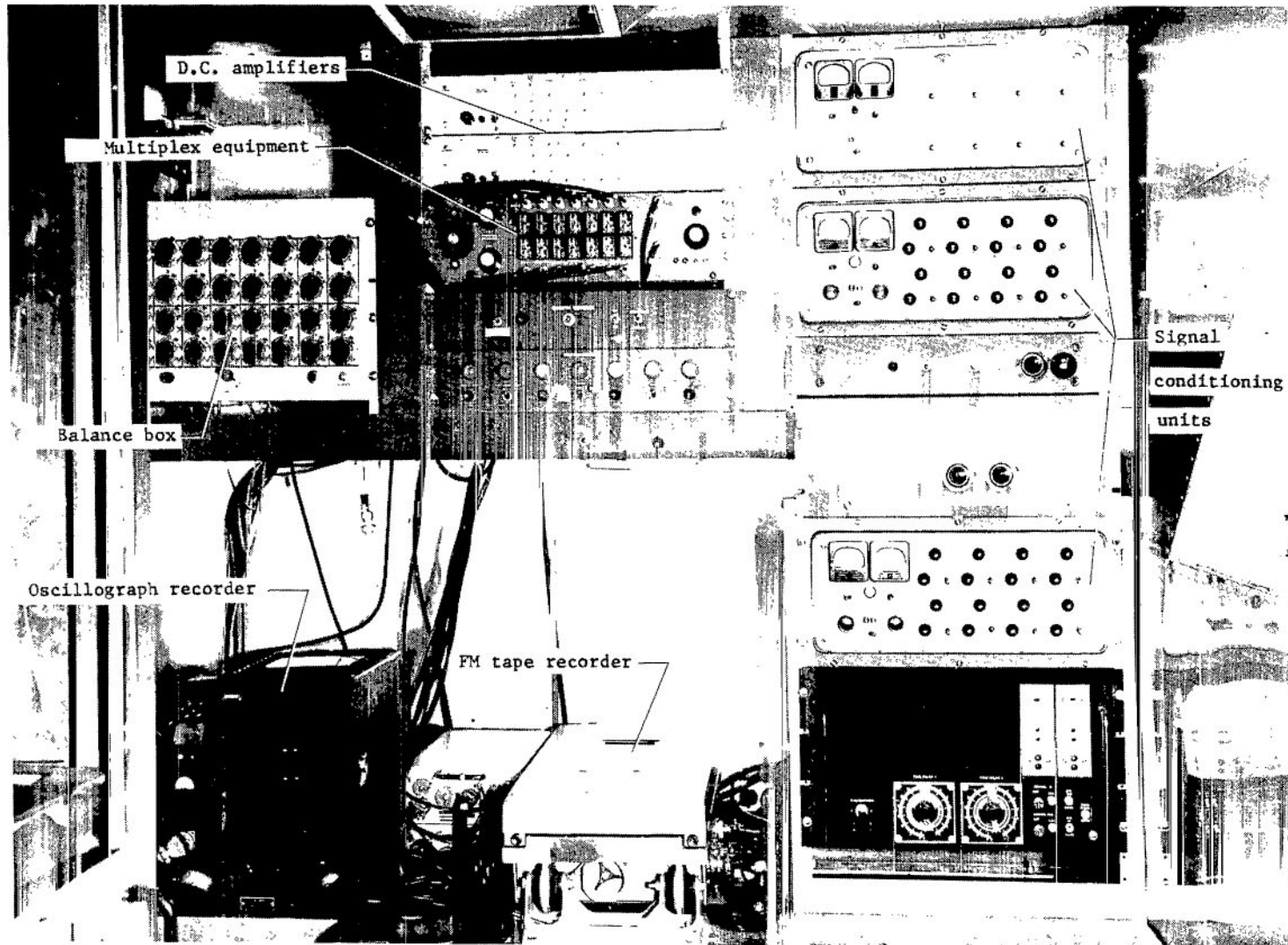


Figure 5.- Interior of instrument compartment on small test carriage.

L-72-2461



L-72-2462

Figure 6.- Self-propelled multiple-pass rotary mixer used in preinstallation soil processing.



Figure 7.- Installation of processed soil in test bed.

L-72-2463

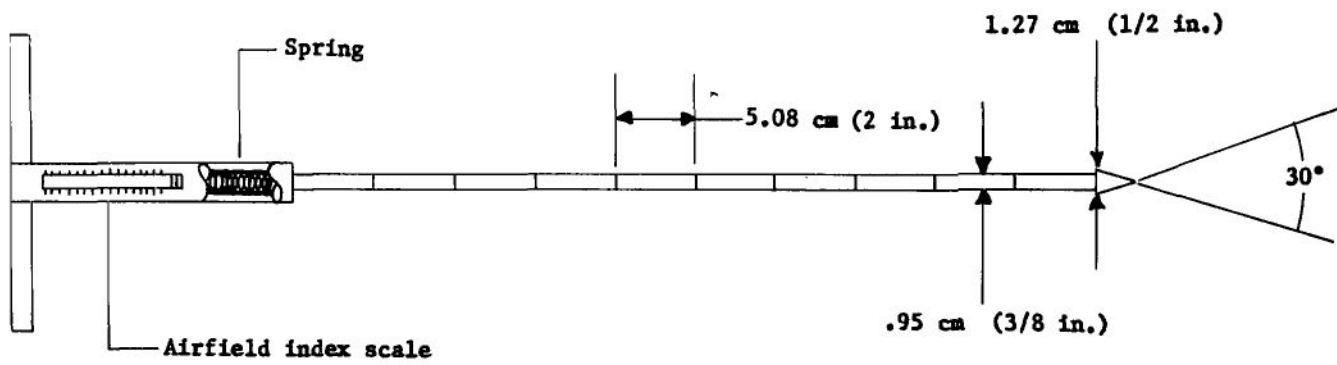


Figure 8.- Schematic of airfield cone penetrometer.



L-72-2464

Figure 9.- Airfield penetrometer test in progress.

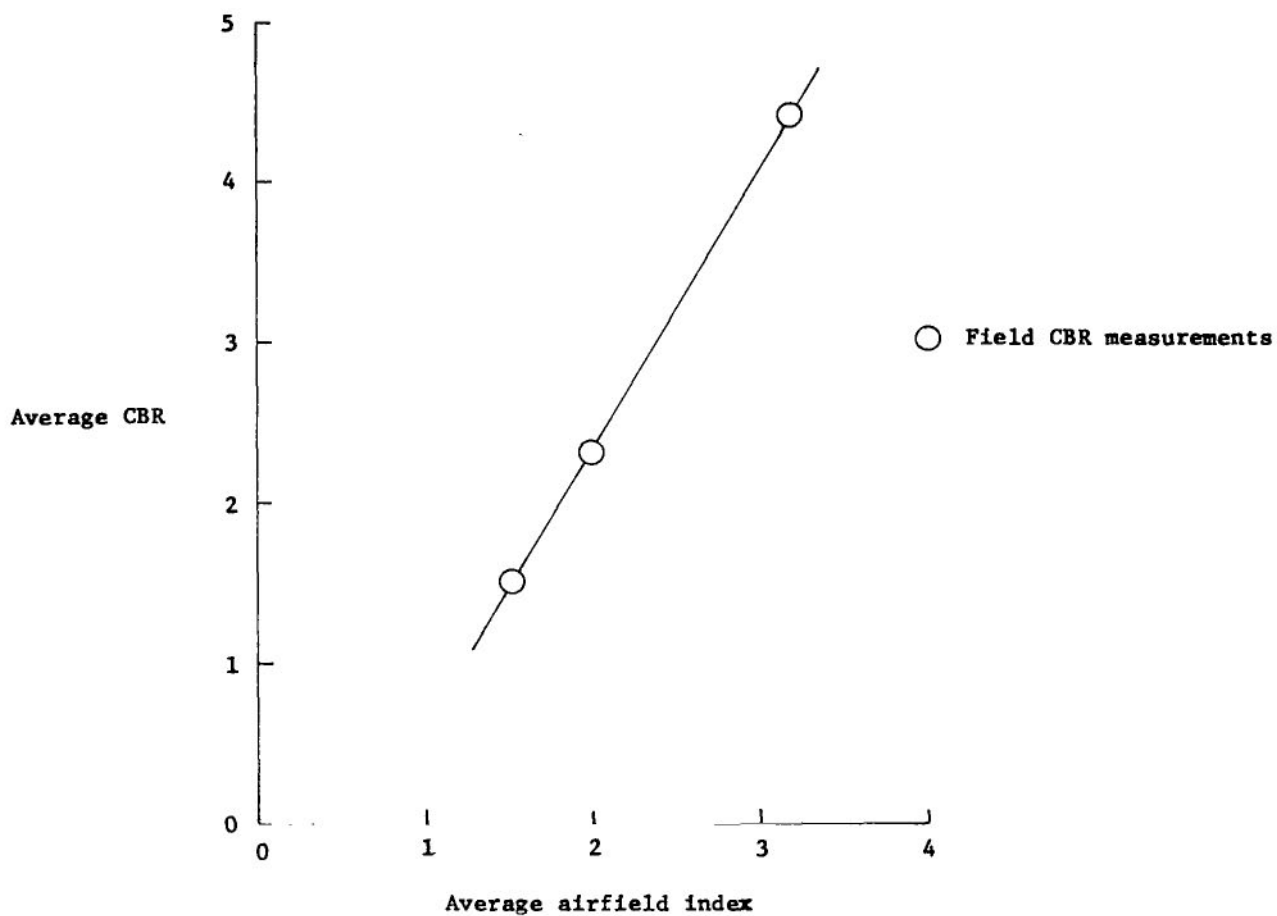


Figure 10.- Correlation of airfield index with California bearing ratio (CBR) for clay. Average values shown for 0 to 15.2 cm (0 to 6 in.) of depth.

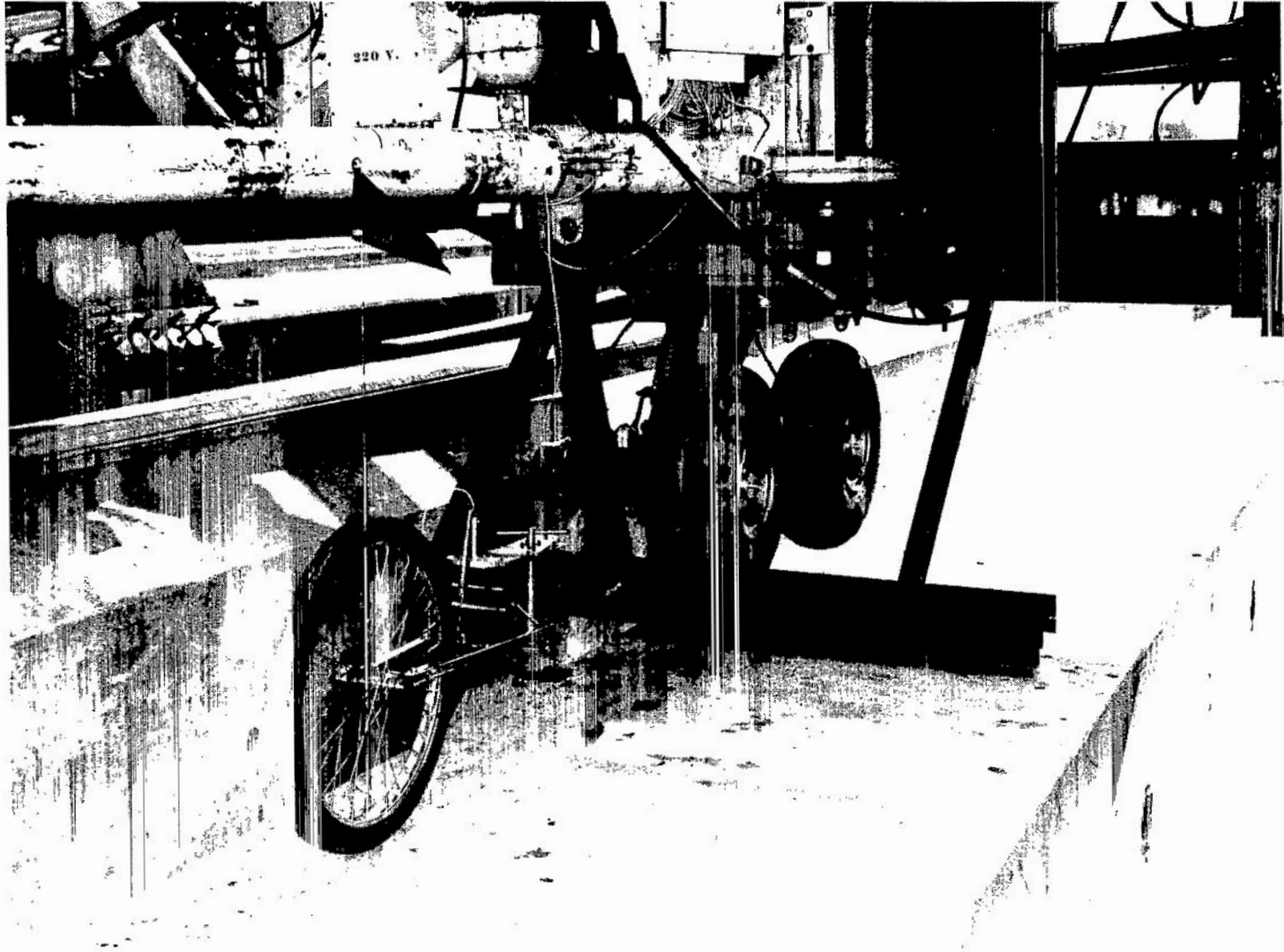
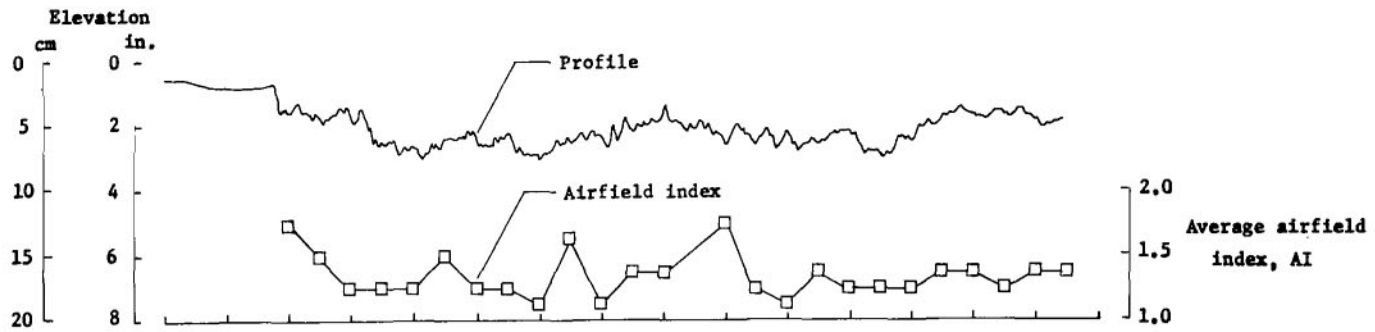
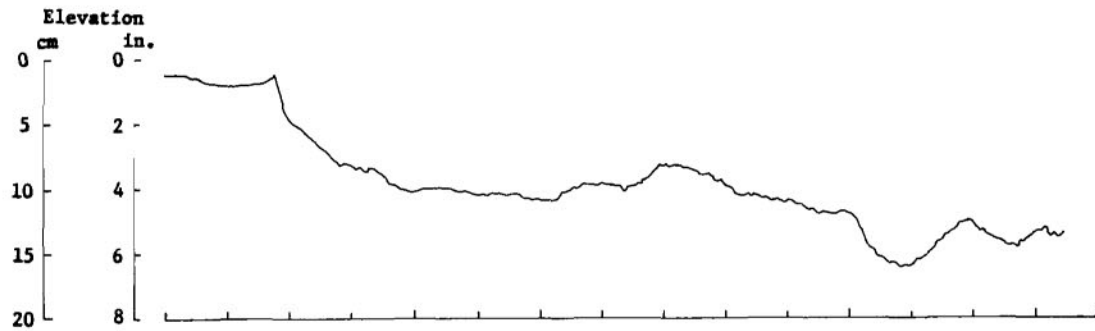


Figure 11.- Continuous-reading profilometer. TAXLE in background.

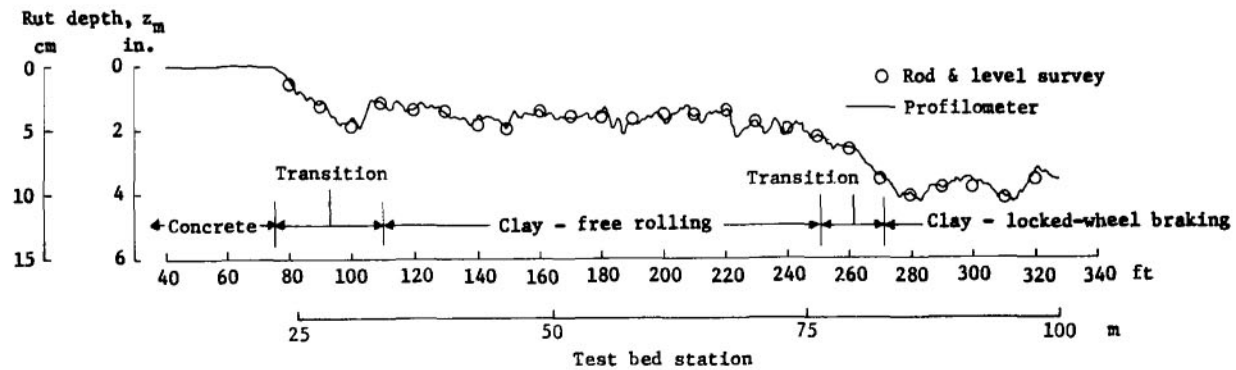
L-69-5533



(a) Profile before test run.



(b) Profile after test run.



(c) Derived rut depth.

Figure 12.- Test-bed profiles before and after a typical test run.

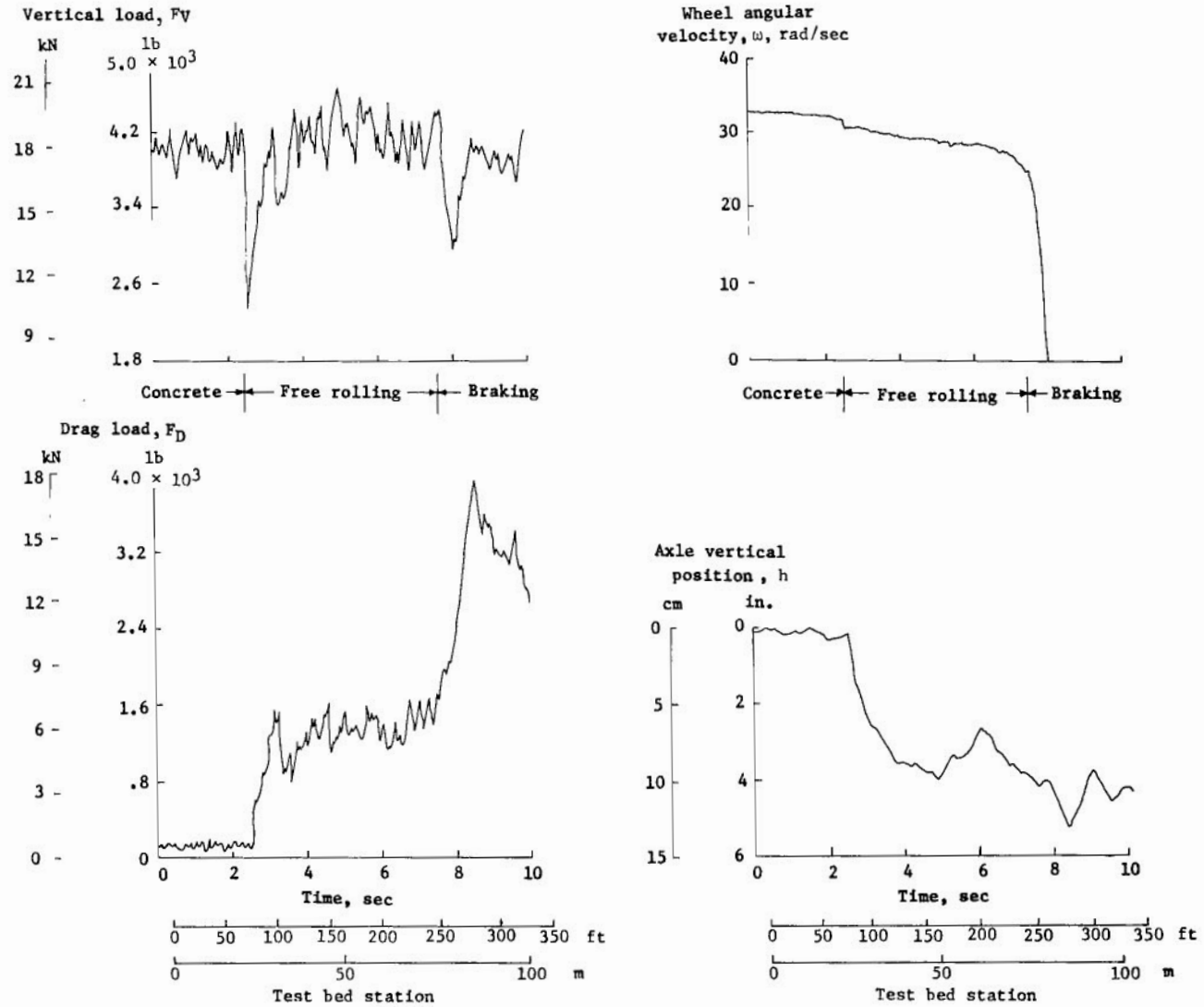


Figure 13.- Time histories for a typical test run. SWDYN; AI 1.5 clay; $p_t = 48 \text{ N/cm}^2$ (70 lb/in²); $V_G = 21$ knots.

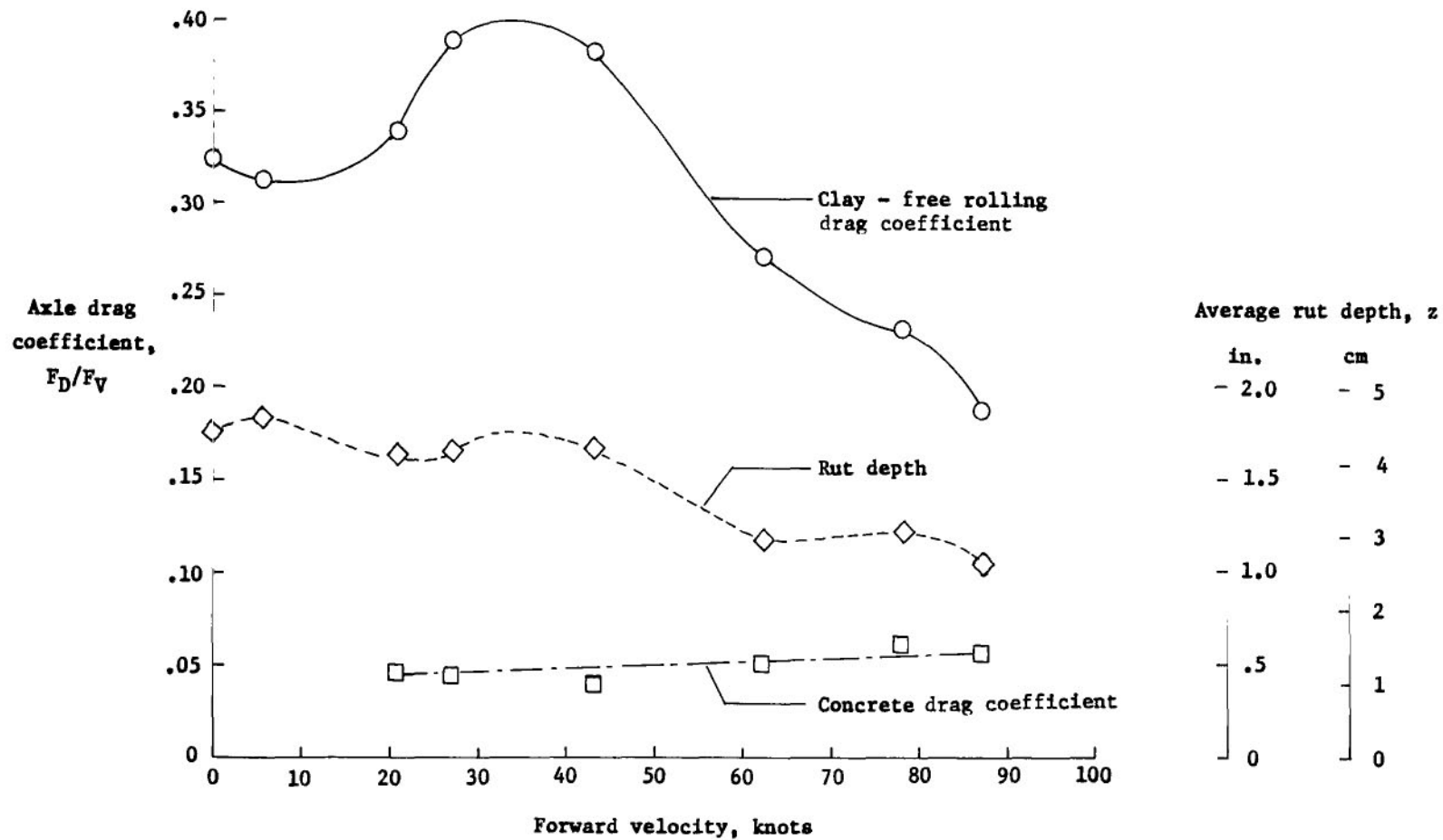
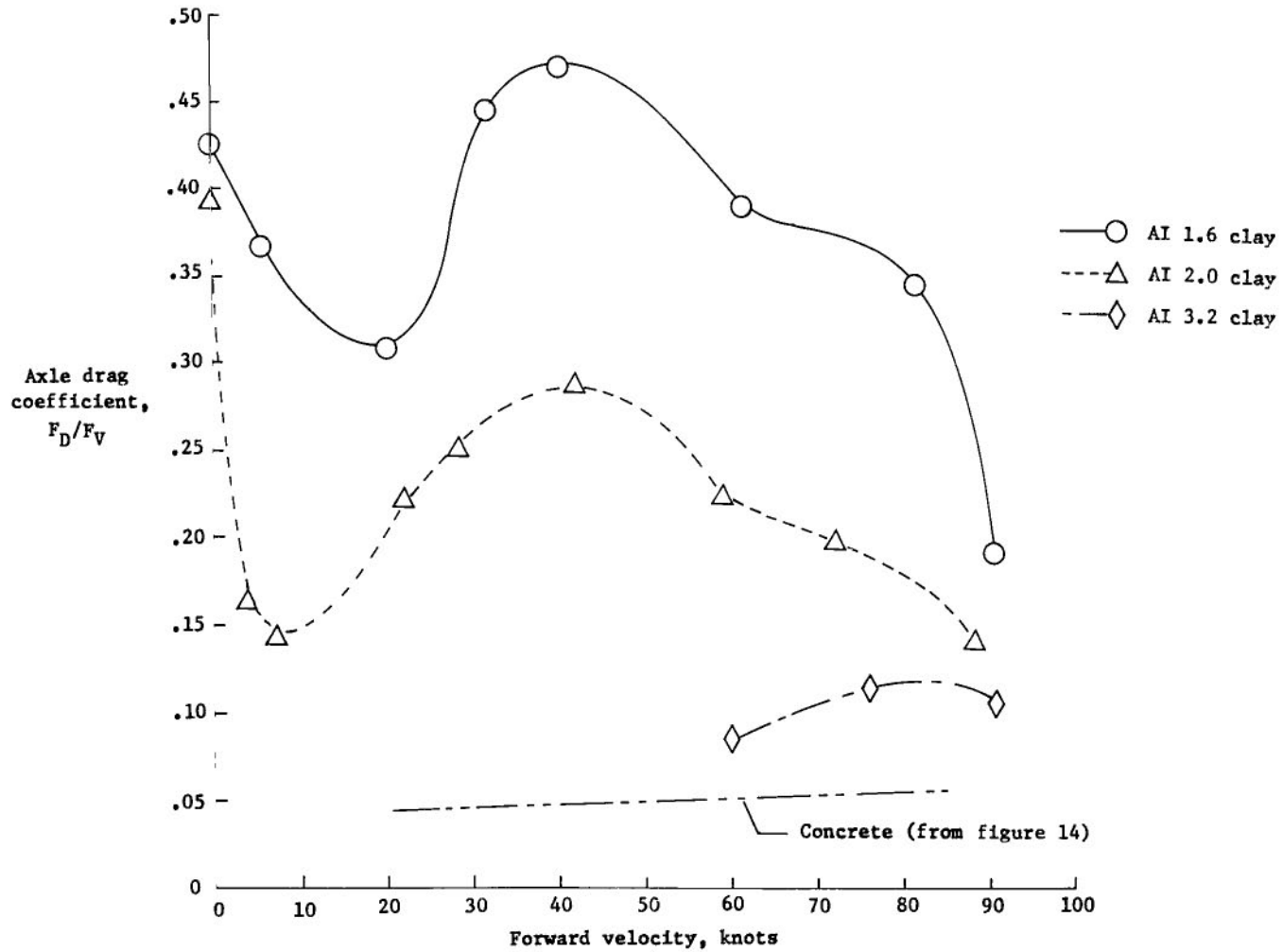


Figure 14.- Axle drag coefficients and rut depths developed by SWDYN. AI 1.5 clay; $p_t = 48 \text{ N/cm}^2$ (70 lb/in²).

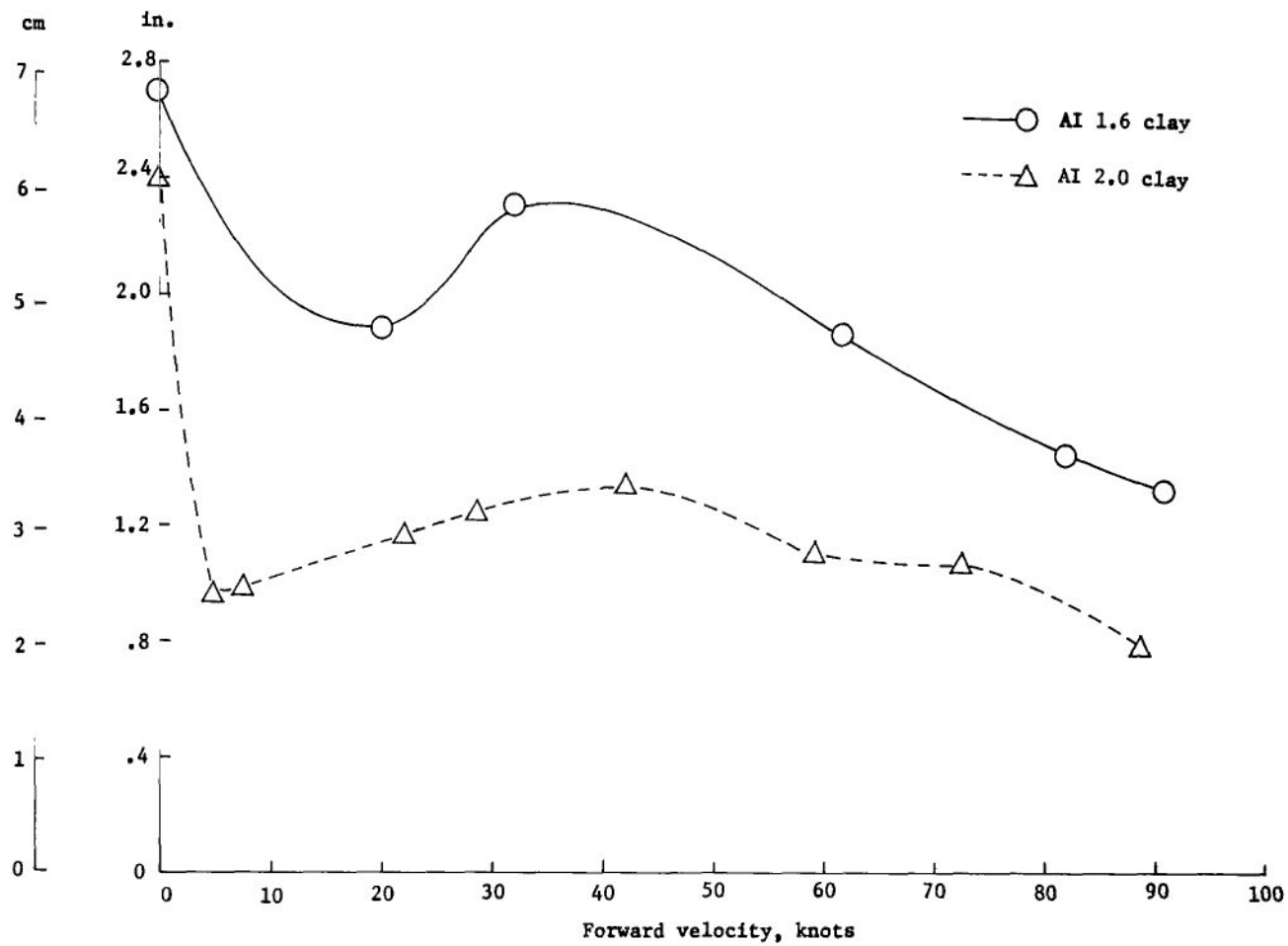


(a) Axle drag coefficients.

Figure 15.- Axle drag coefficients and rut depths developed by SAXLE in several different soil strengths.

$$p_t = 48 \text{ N/cm}^2 \text{ (70 lb/in}^2\text{)}.$$

Average rut depth, z



(b) Rut depths.

Figure 15.- Concluded.

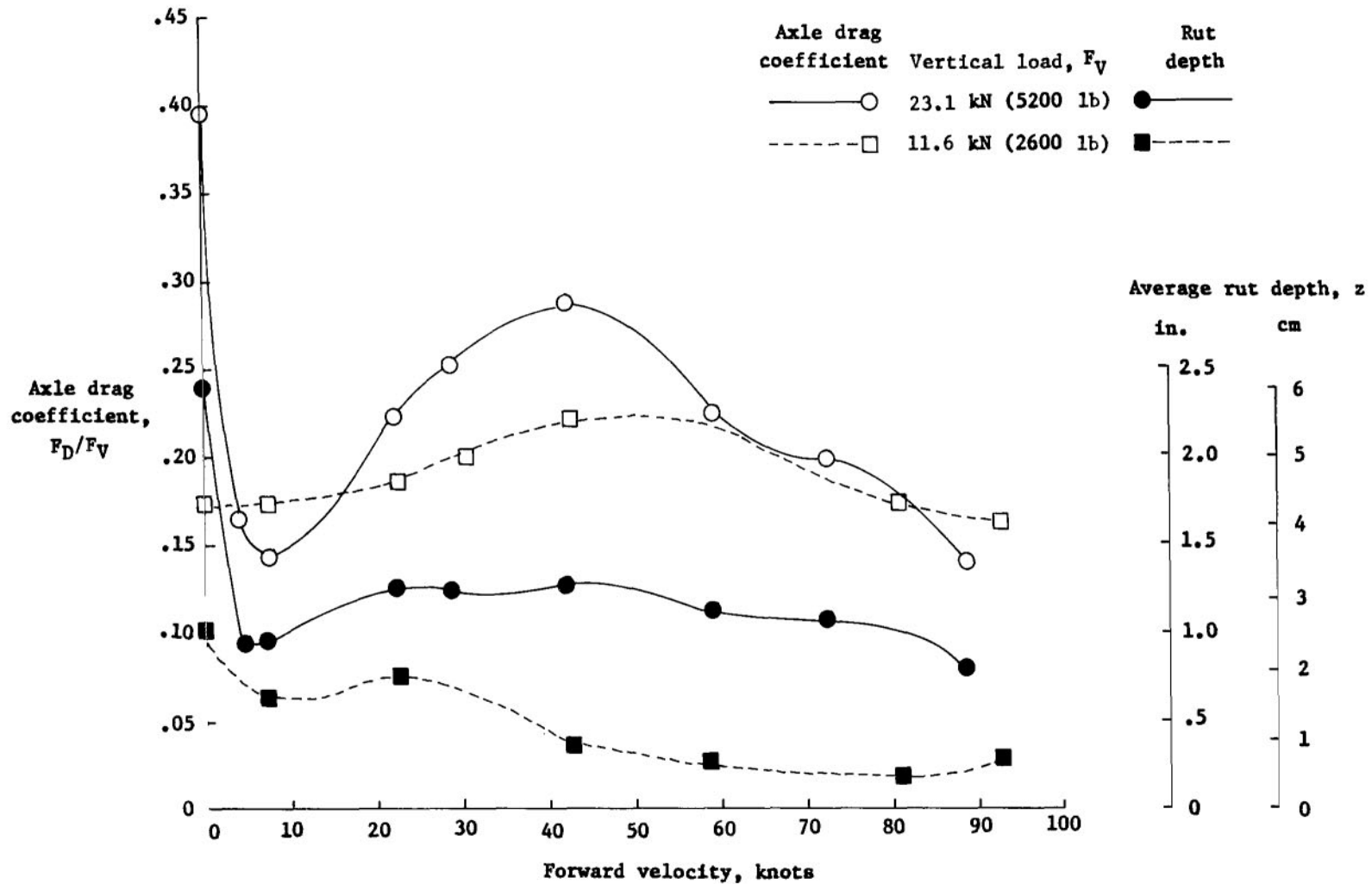
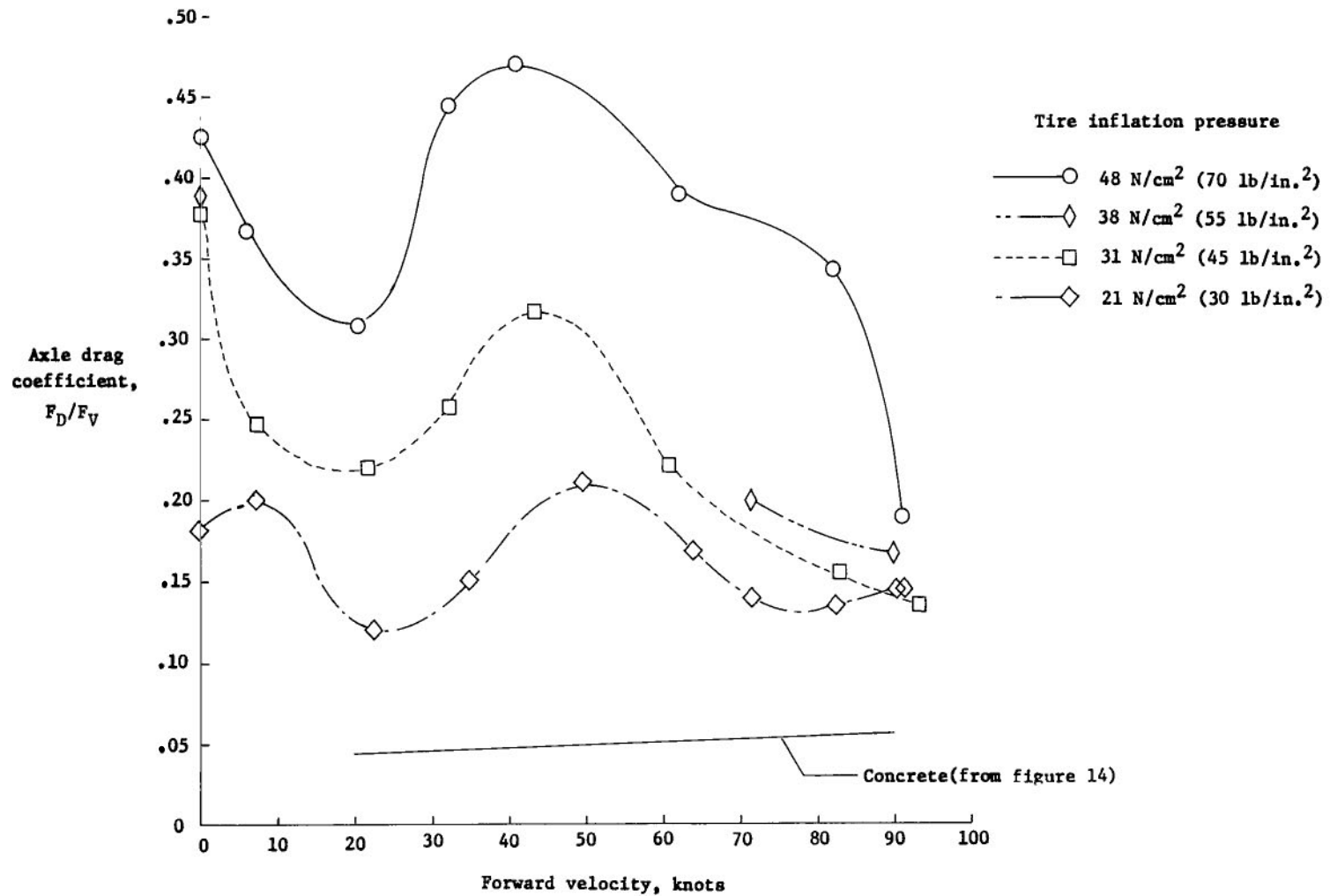


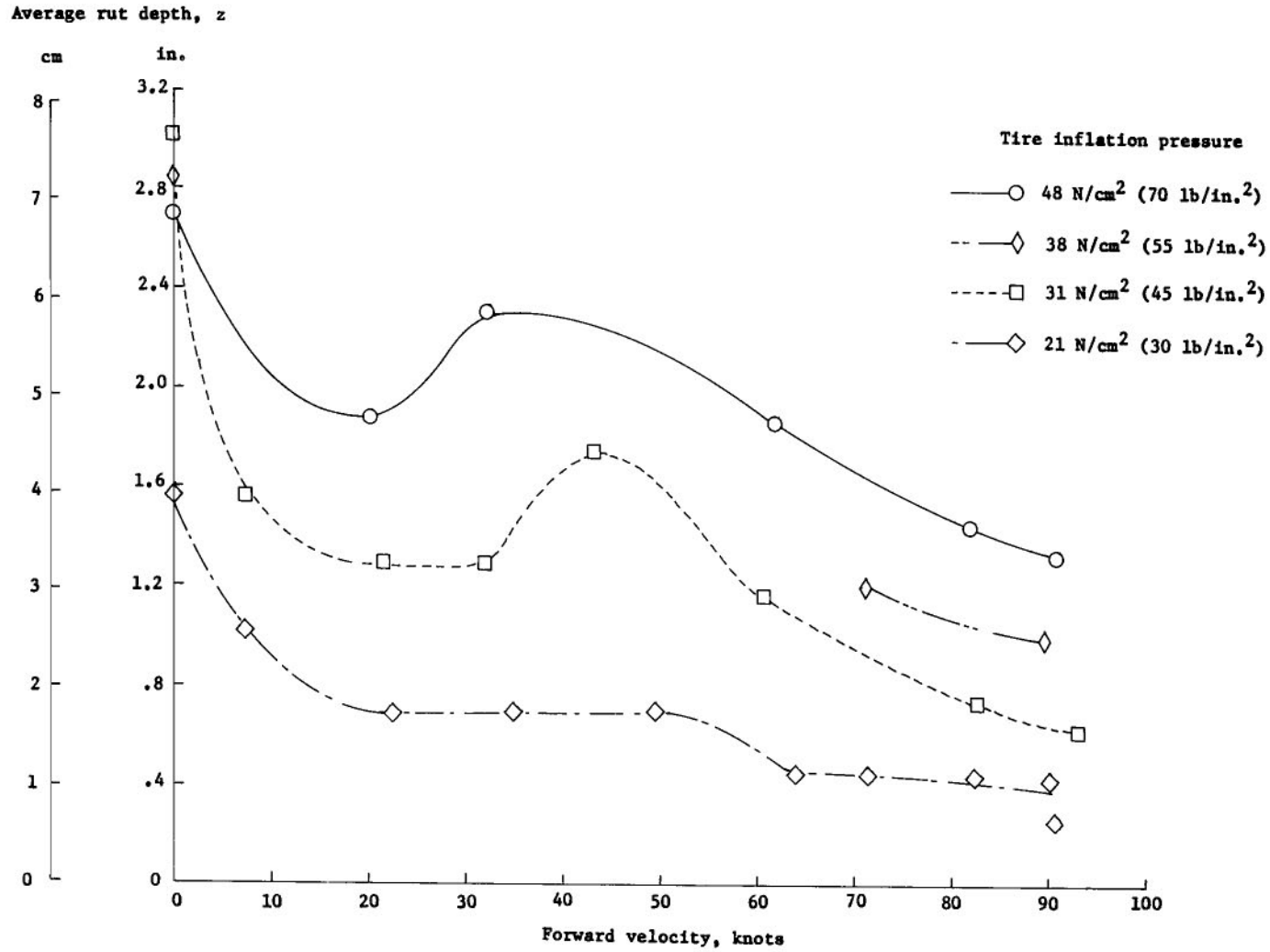
Figure 16.- Axle drag coefficients and rut depths developed by SAXLE at two different vertical loads.

AI 2.0 clay; $p_t = 48 \text{ N/cm}^2$ (70 lb/in²).



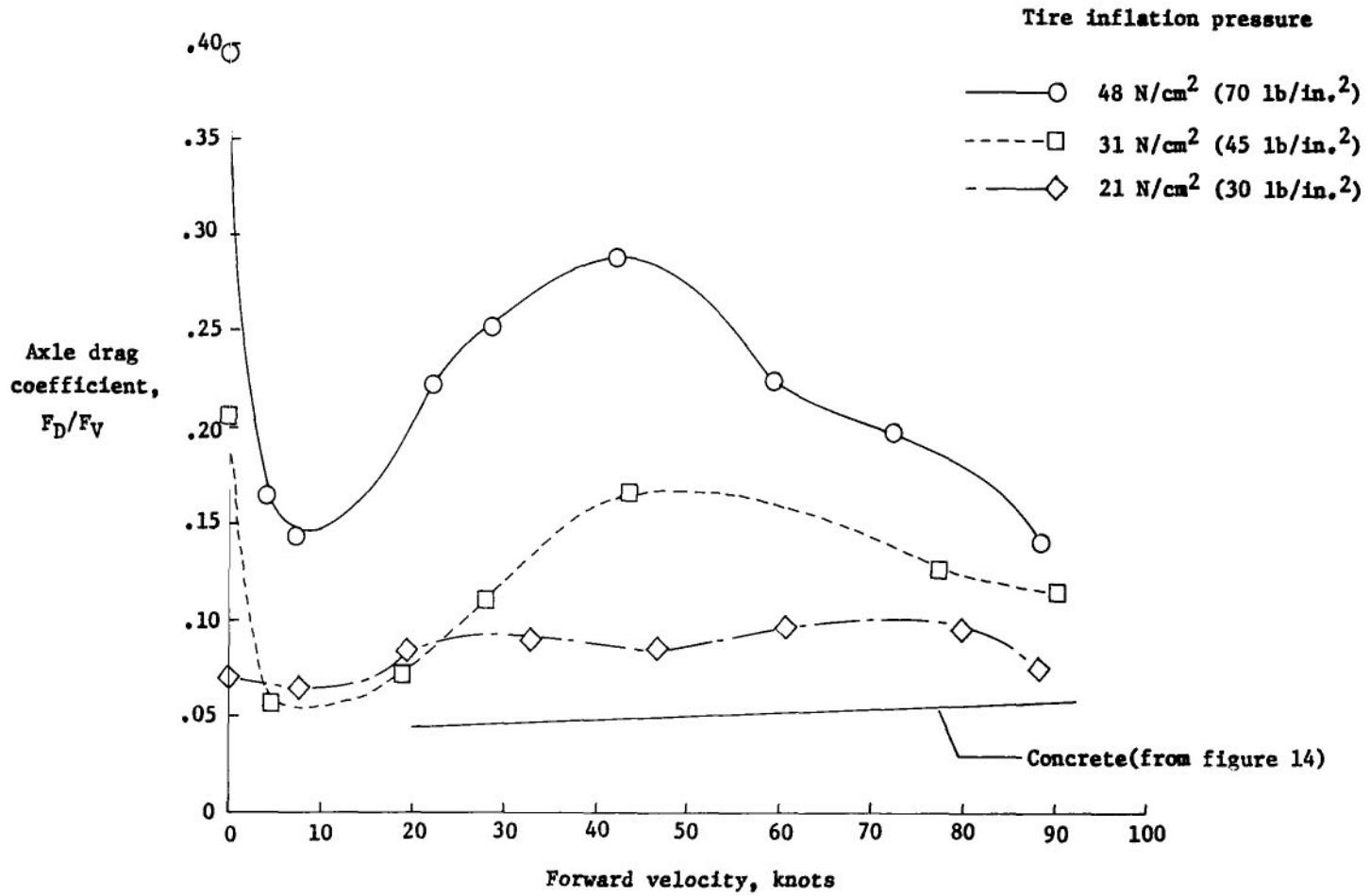
(a) Axle drag coefficients.

Figure 17.- Axle drag coefficients and rut depths developed by SAXLE at four different tire inflation pressures. AI 1.6 clay.



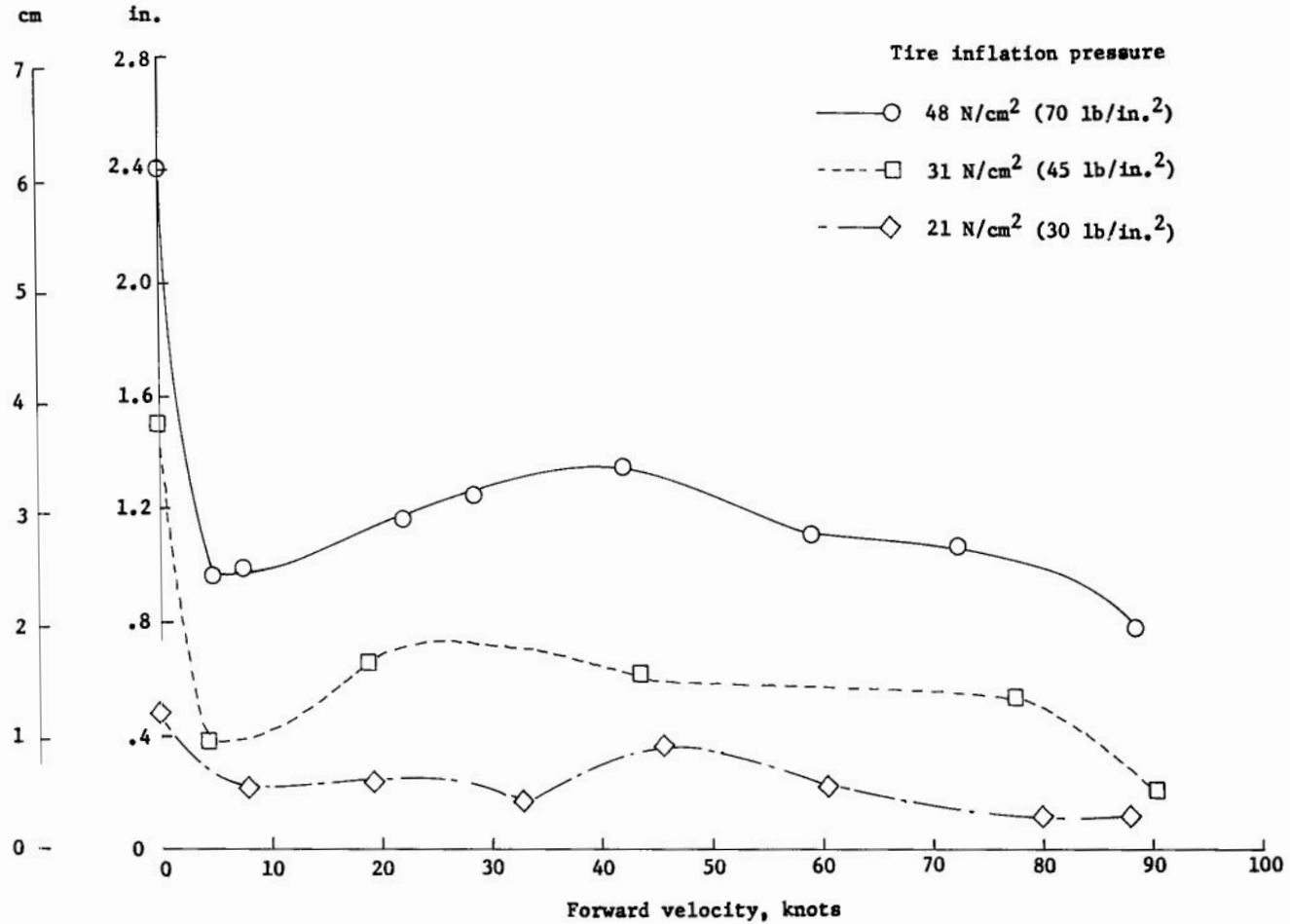
(b) Rut depths.

Figure 17.- Concluded.



(a) Axle drag coefficients.

Figure 18.- Axle drag coefficients and rut depths developed by SAXLE at three different tire inflation pressures. AI 2.0 clay.

Average rut depth, z 

(b) Rut depths.

Figure 18.- Concluded.

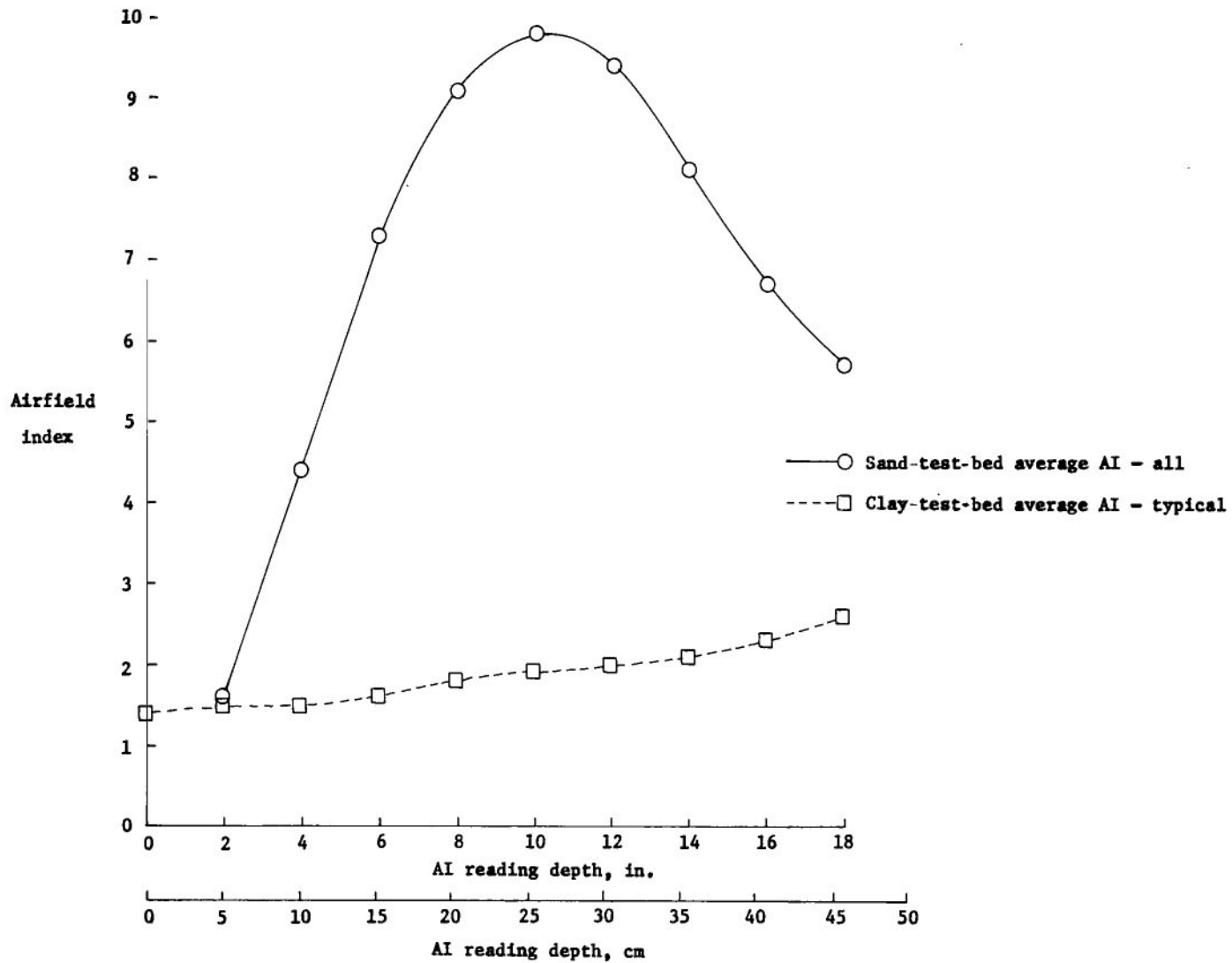
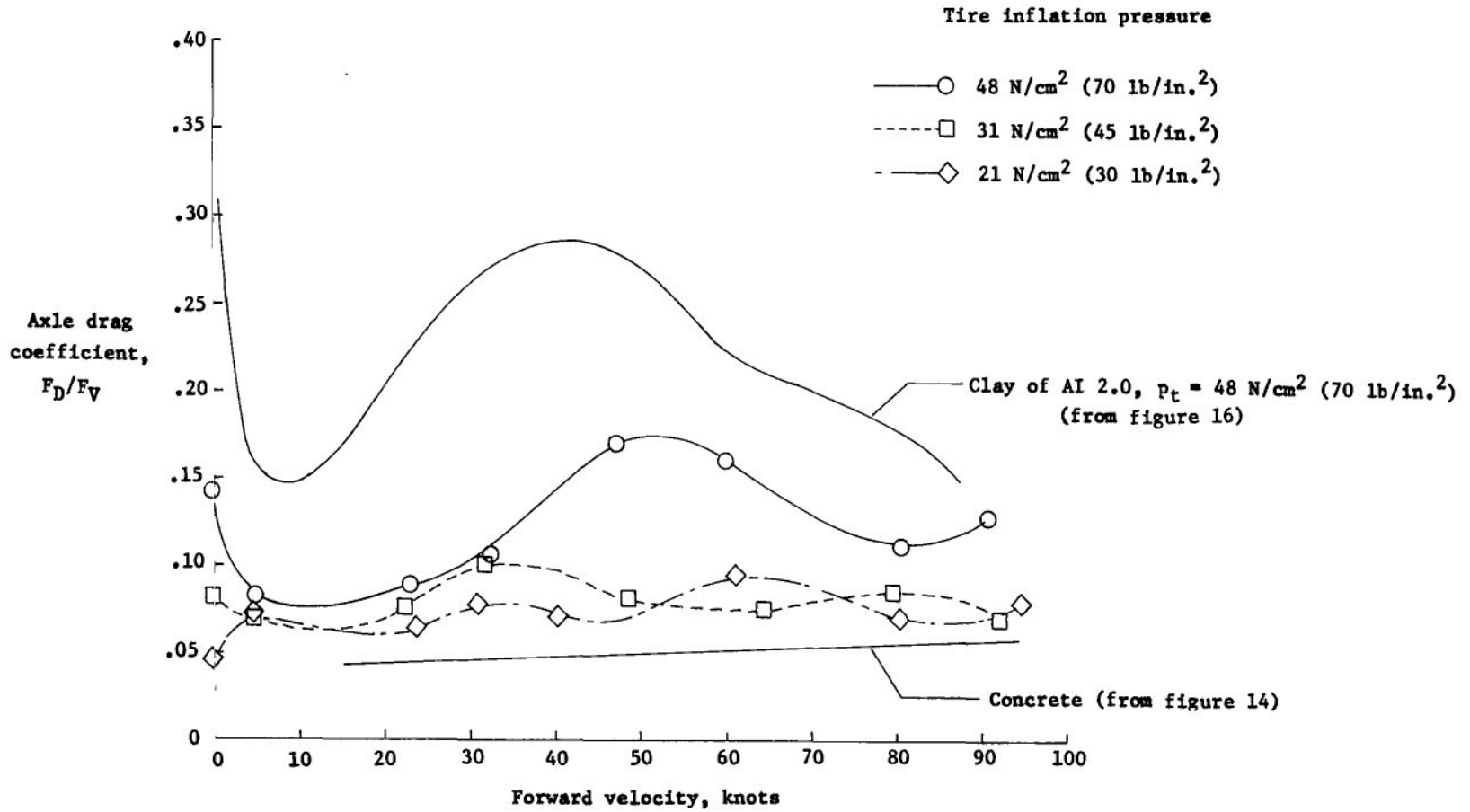


Figure 19.- Variation of airfield index with depth for sand and for clay.



(a) Axle drag coefficients.

Figure 20.- Axle drag coefficients and rut depths developed in sand by SAXLE at three different tire inflation pressures.

Average rut depth, z

cm in.

7- 2.8-

6- 2.4-

5- 2.0-

4- 1.6-

3- 1.2-

2- .8-

1- .4-

0 0

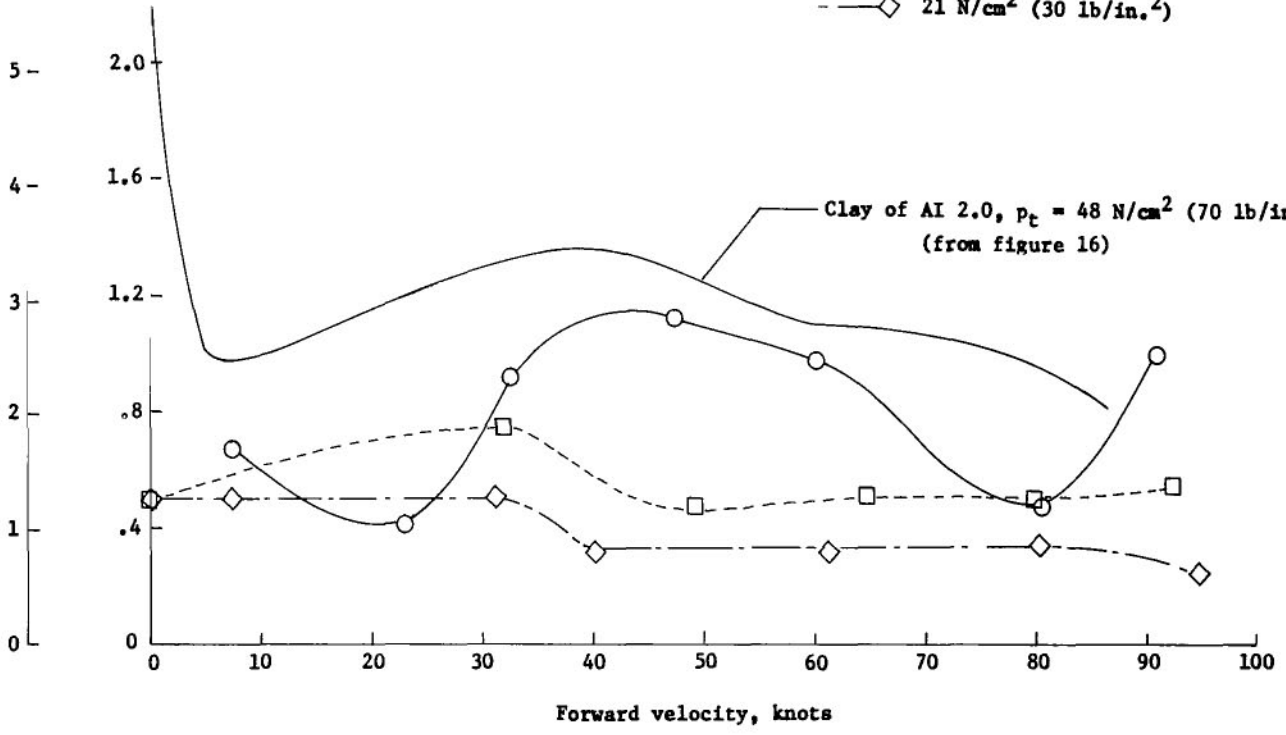
Tire inflation pressure

—○ 48 N/cm² (70 lb/in.²)

- - -□ 31 N/cm² (45 lb/in.²)

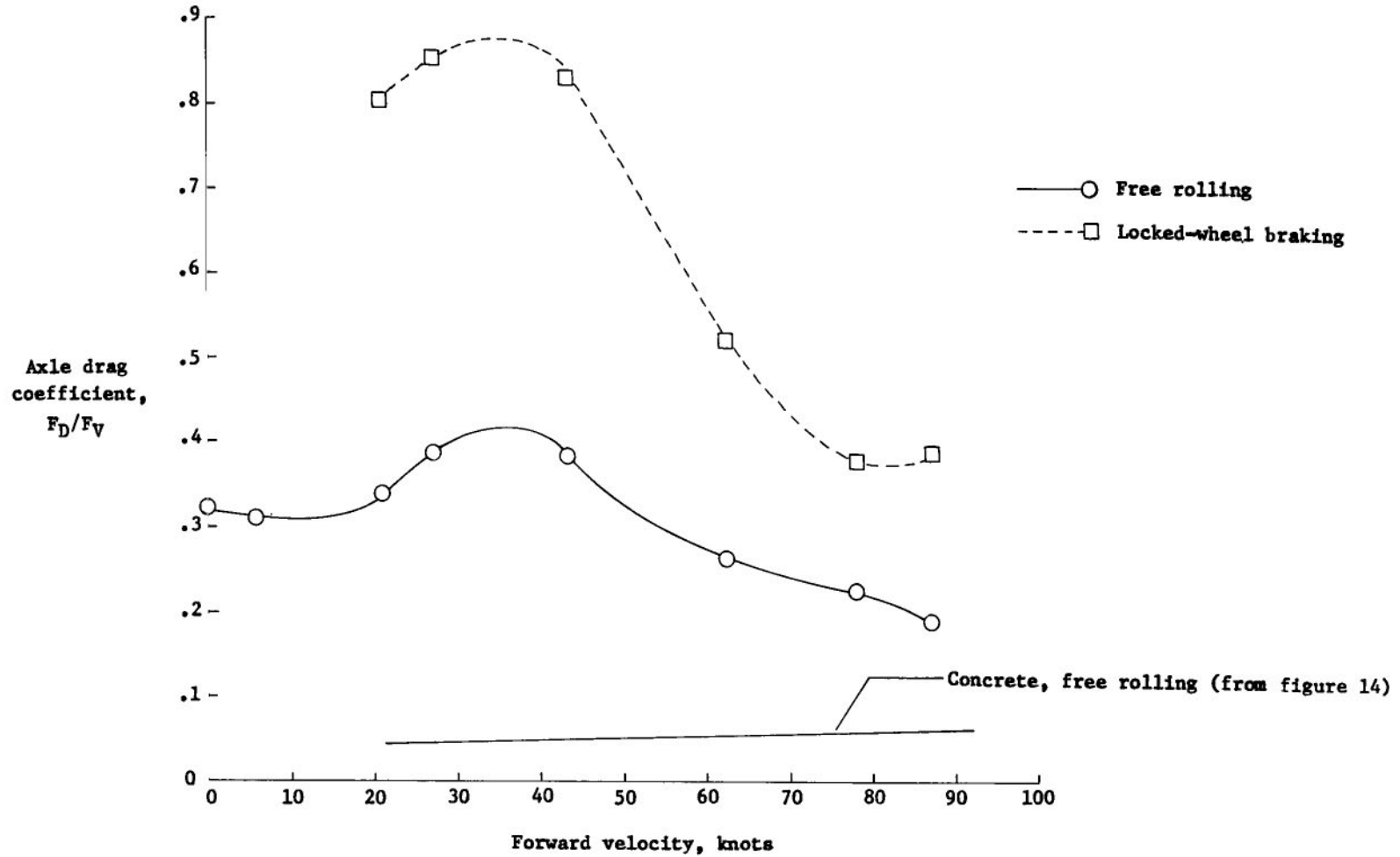
- - -◇ 21 N/cm² (30 lb/in.²)

Clay of AI 2.0, p_t = 48 N/cm² (70 lb/in.²)
(from figure 16)



(b) Rut depths.

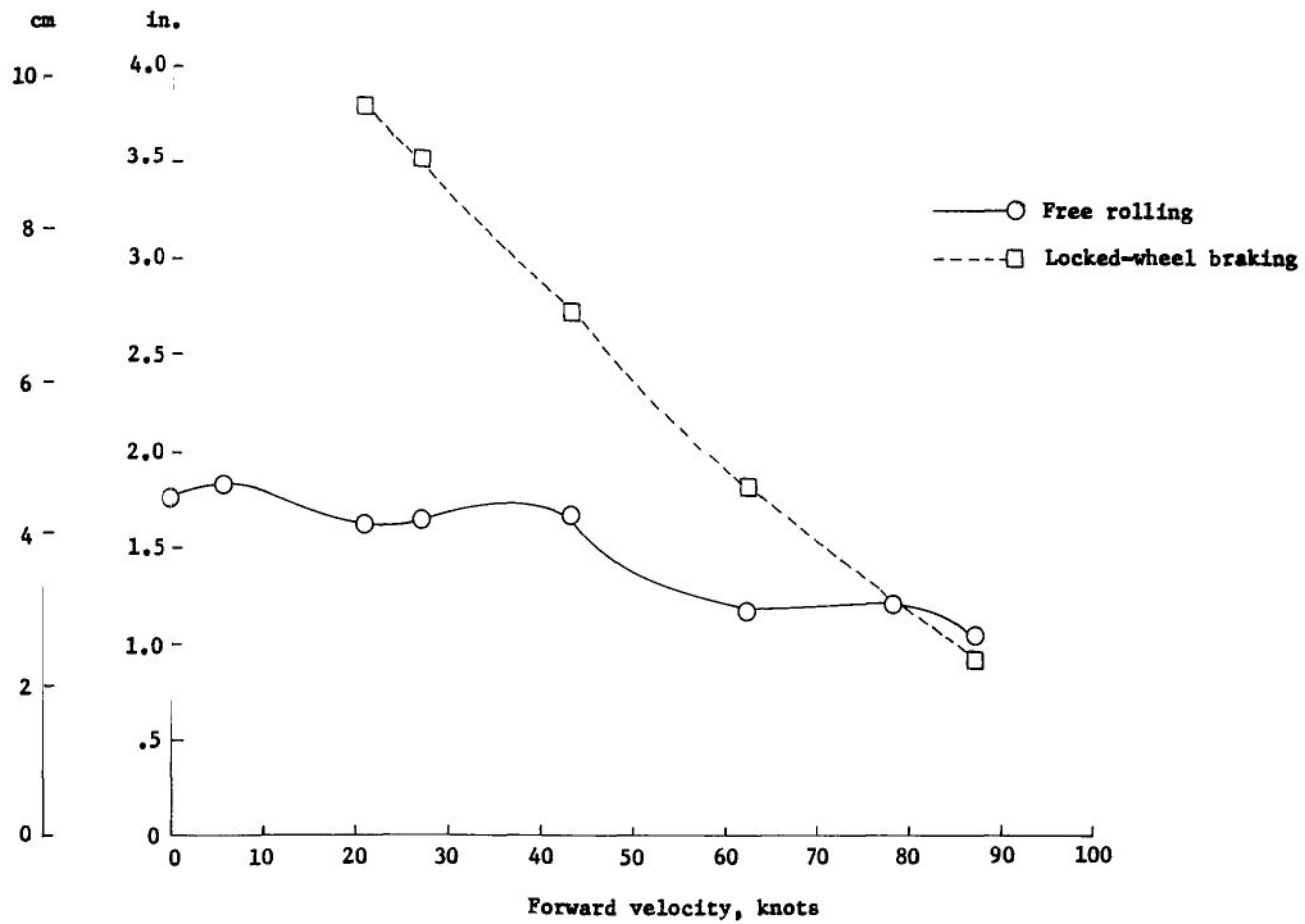
Figure 20.- Concluded.



(a) Axle drag coefficients.

Figure 21.- Axle drag coefficients and rut depths for SWDYN locked-wheel braking compared to free rolling on AI 1.5 clay. $p_t = 48 \text{ N/cm}^2$ (70 lb/in²).

Average rut depth, z



(b) Rut depths.

Figure 21.- Concluded.

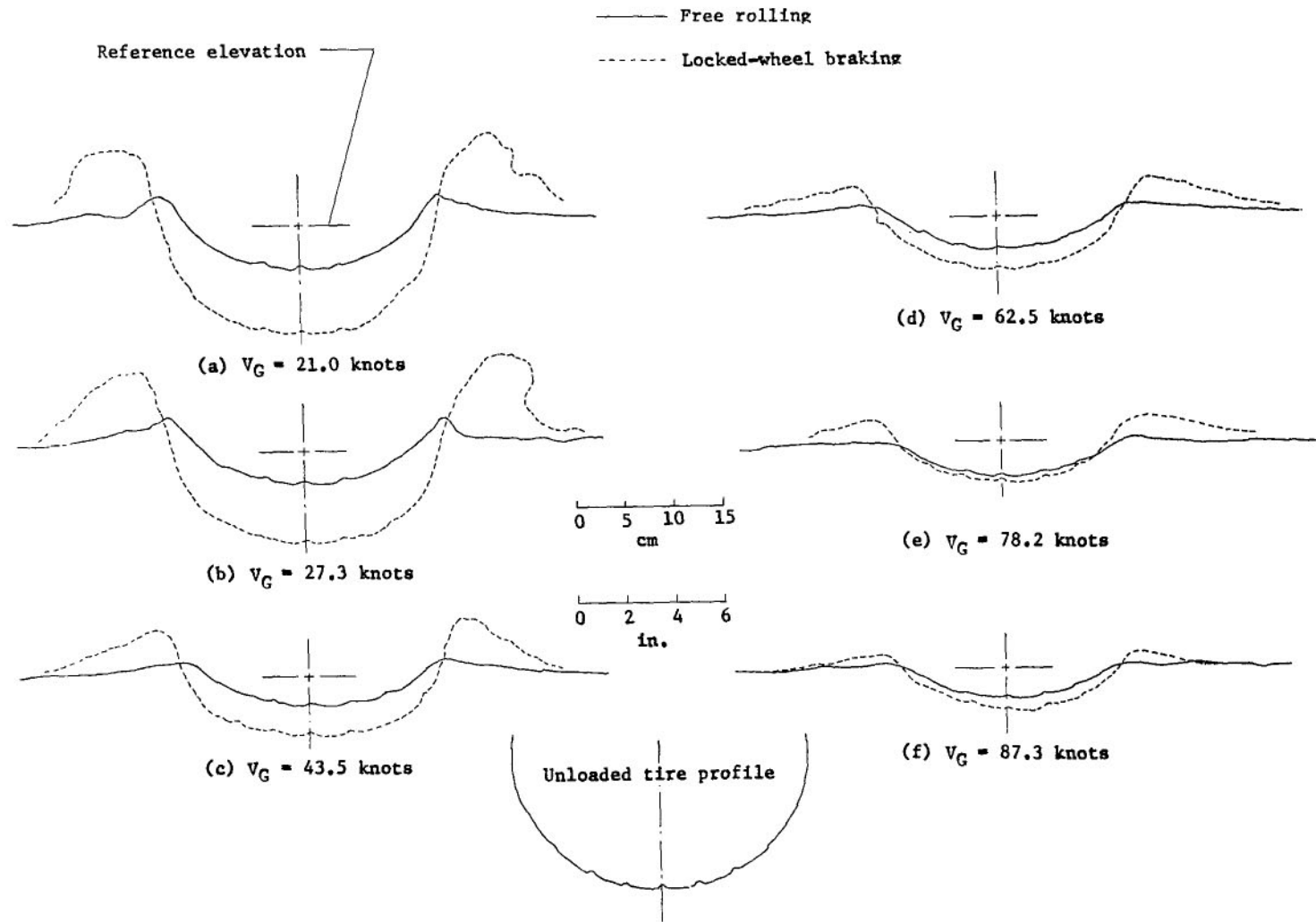
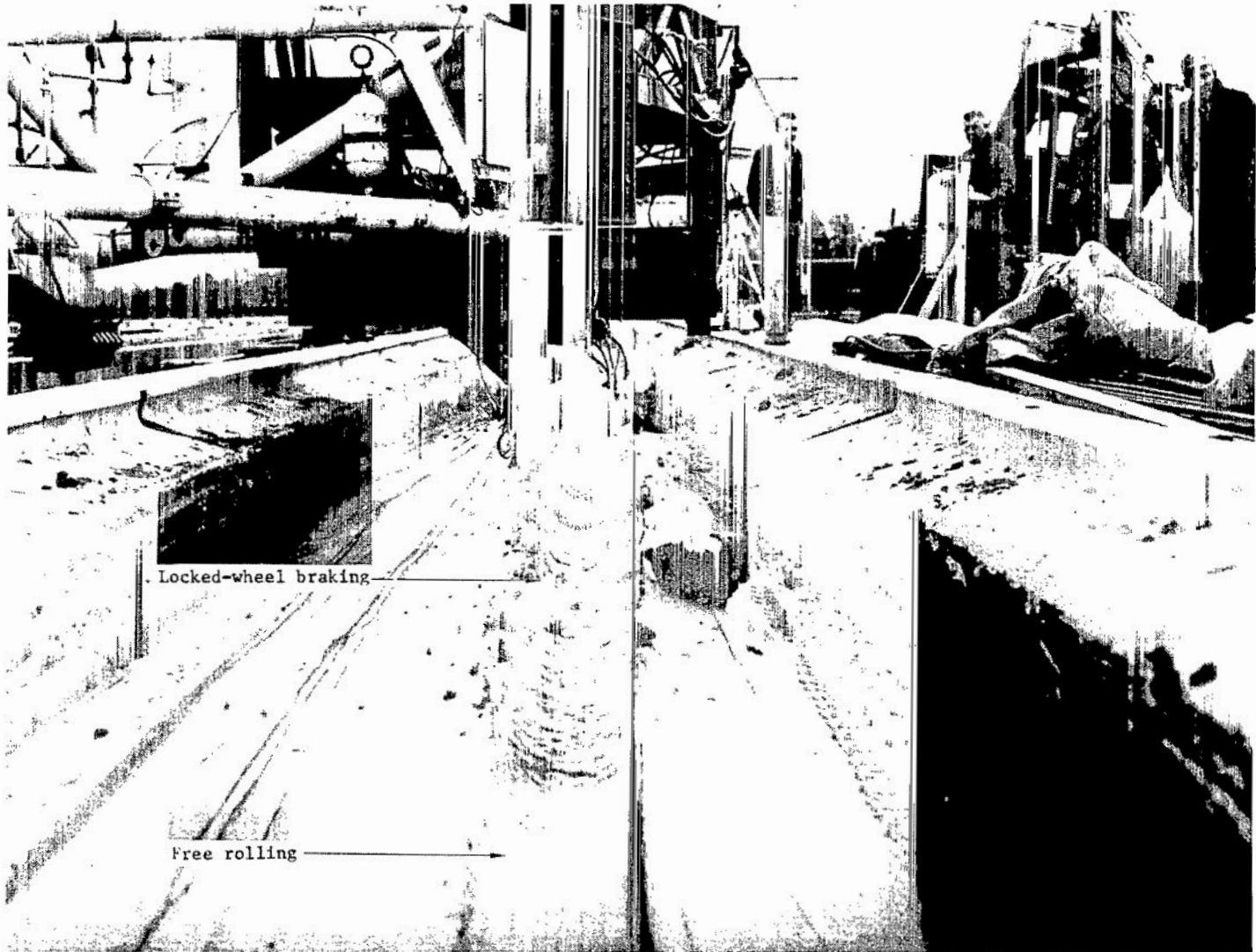
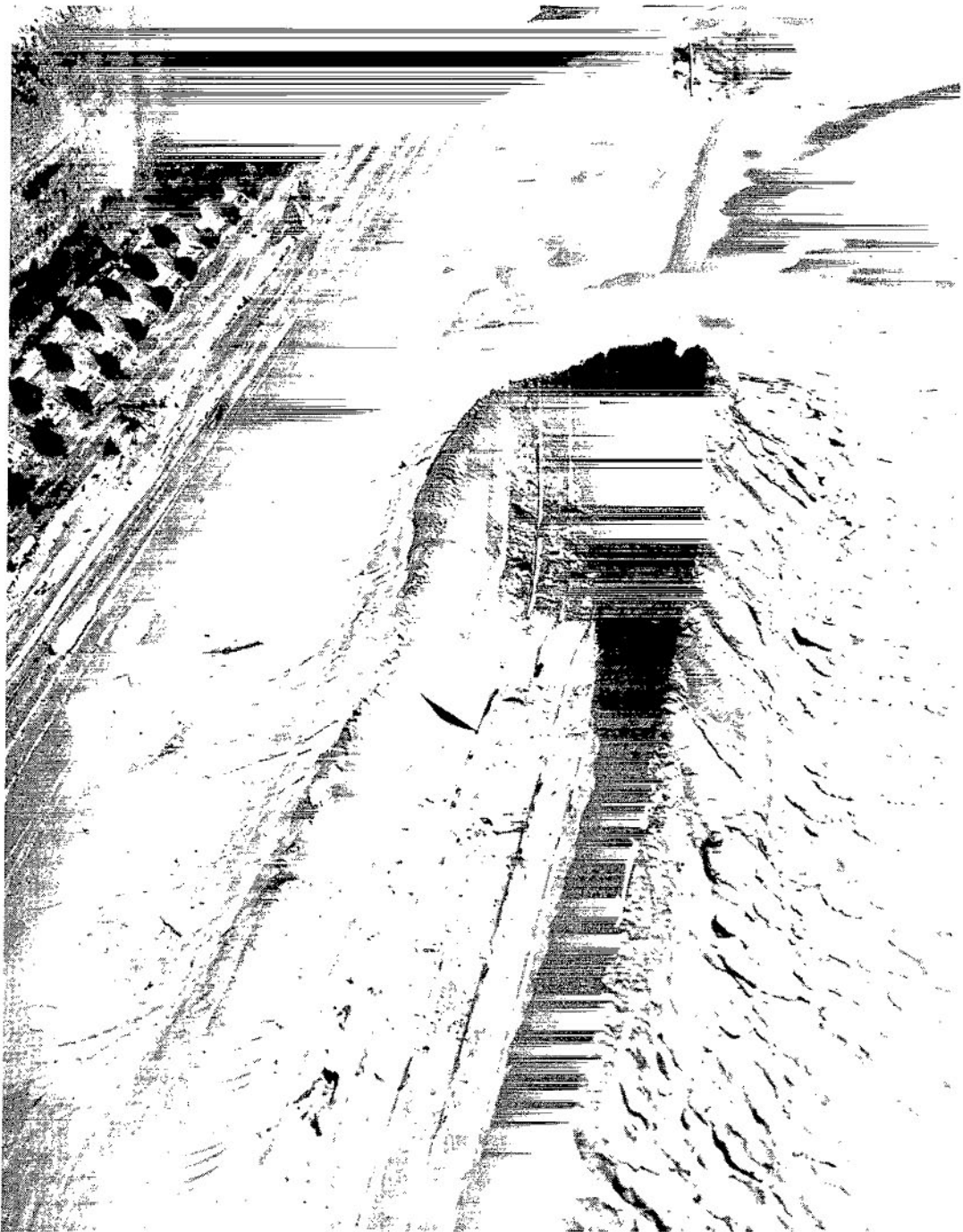


Figure 22.- Rut cross-sectional profiles created by free rolling and locked-wheel braking of SWDYN.
 AI 1.5 clay; $p_t = 48 \text{ N/cm}^2$ (70 lb/in²).



L-72-2465

Figure 23.- Typical tire ruts in clay, showing transition from free rolling to locked-wheel braking.



L-69-6973

Figure 24.- Bow wave following low-speed tow of SWDYN. AI 1.5 clay.



L-72-2466

Figure 25.- Free rolling and braking ruts in sand test bed.

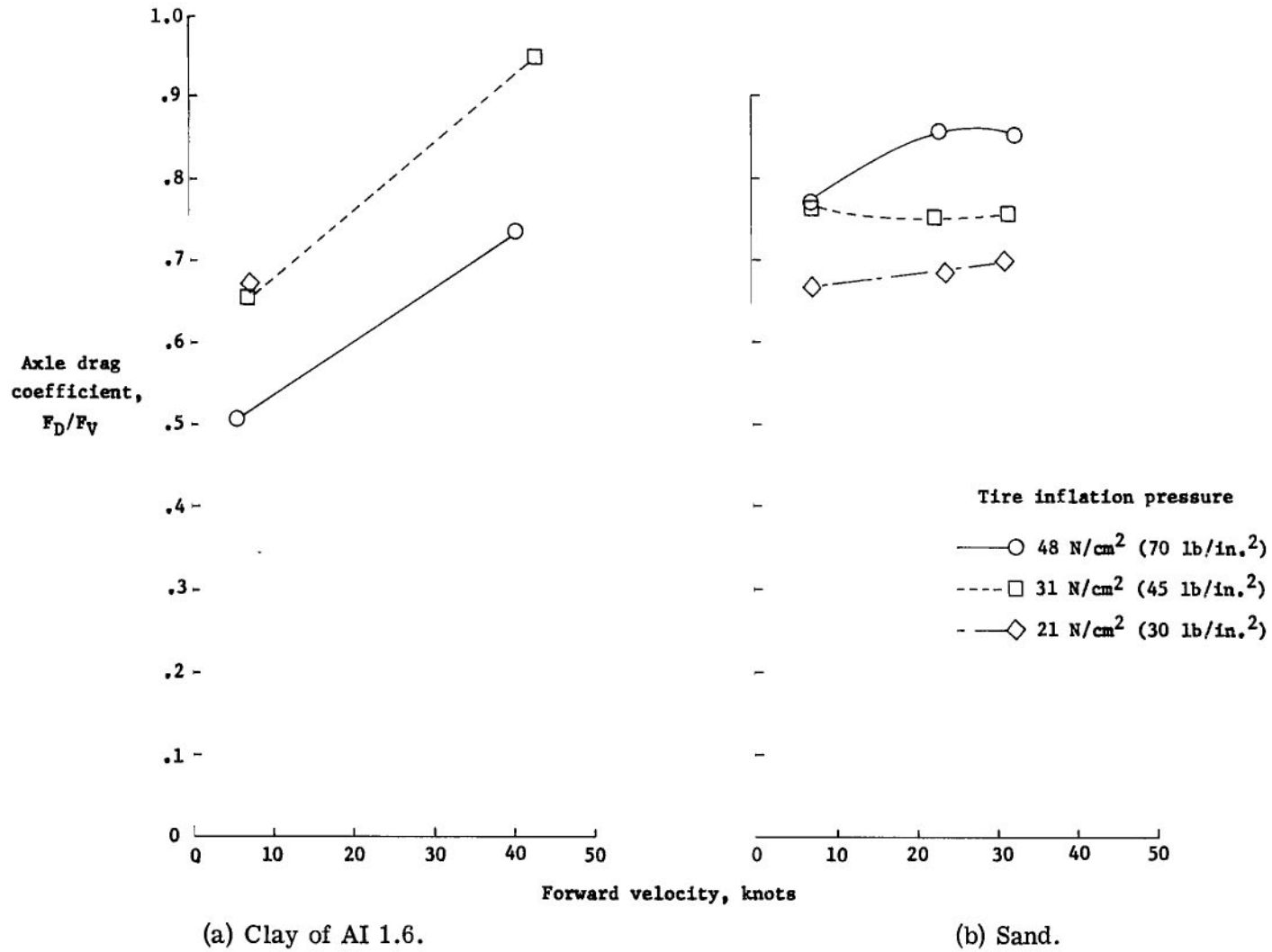
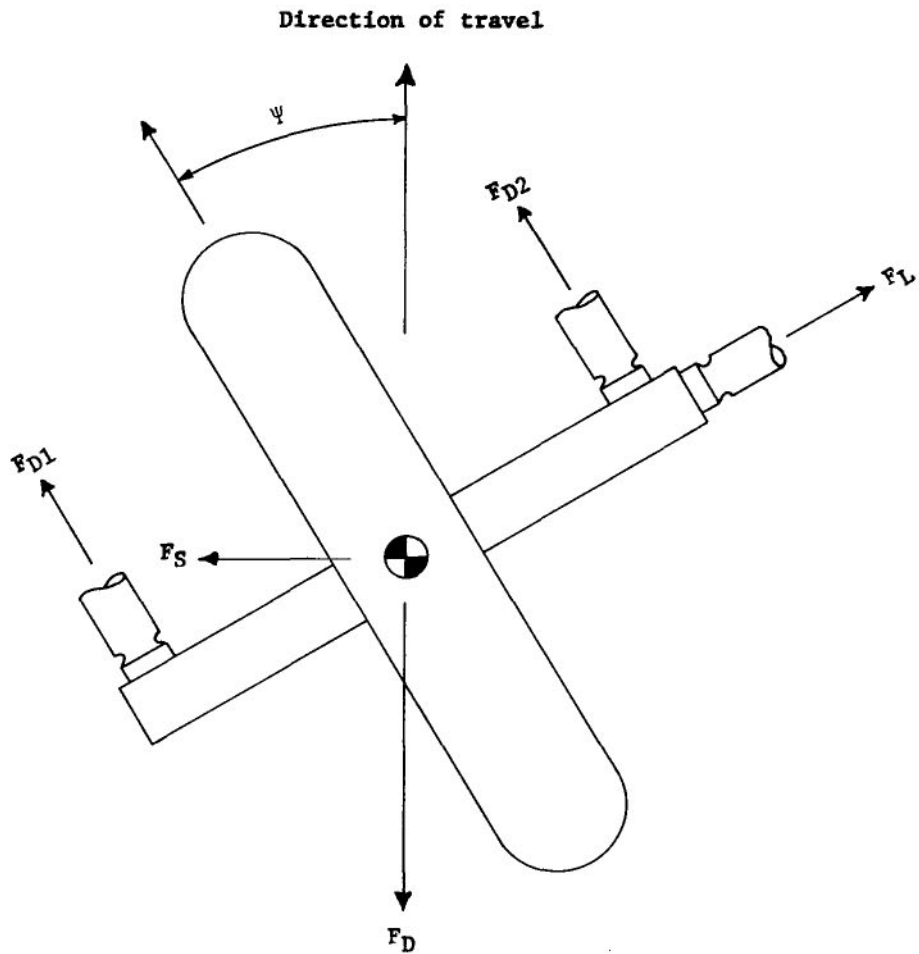


Figure 26.- Locked-wheel braking drag coefficients developed by SAXLE in clay and sand test beds.



L-72-2467

Figure 27.- Typical wheel spin-up area in clay test bed.



$$F_D = F_{D1} \cos \psi + F_{D2} \cos \psi + F_L \sin \psi$$

$$F_S = F_L \cos \psi - F_{D1} \sin \psi - F_{D2} \sin \psi$$

Figure 28.- Schematic of forces on SWDYN during yawed rolling.

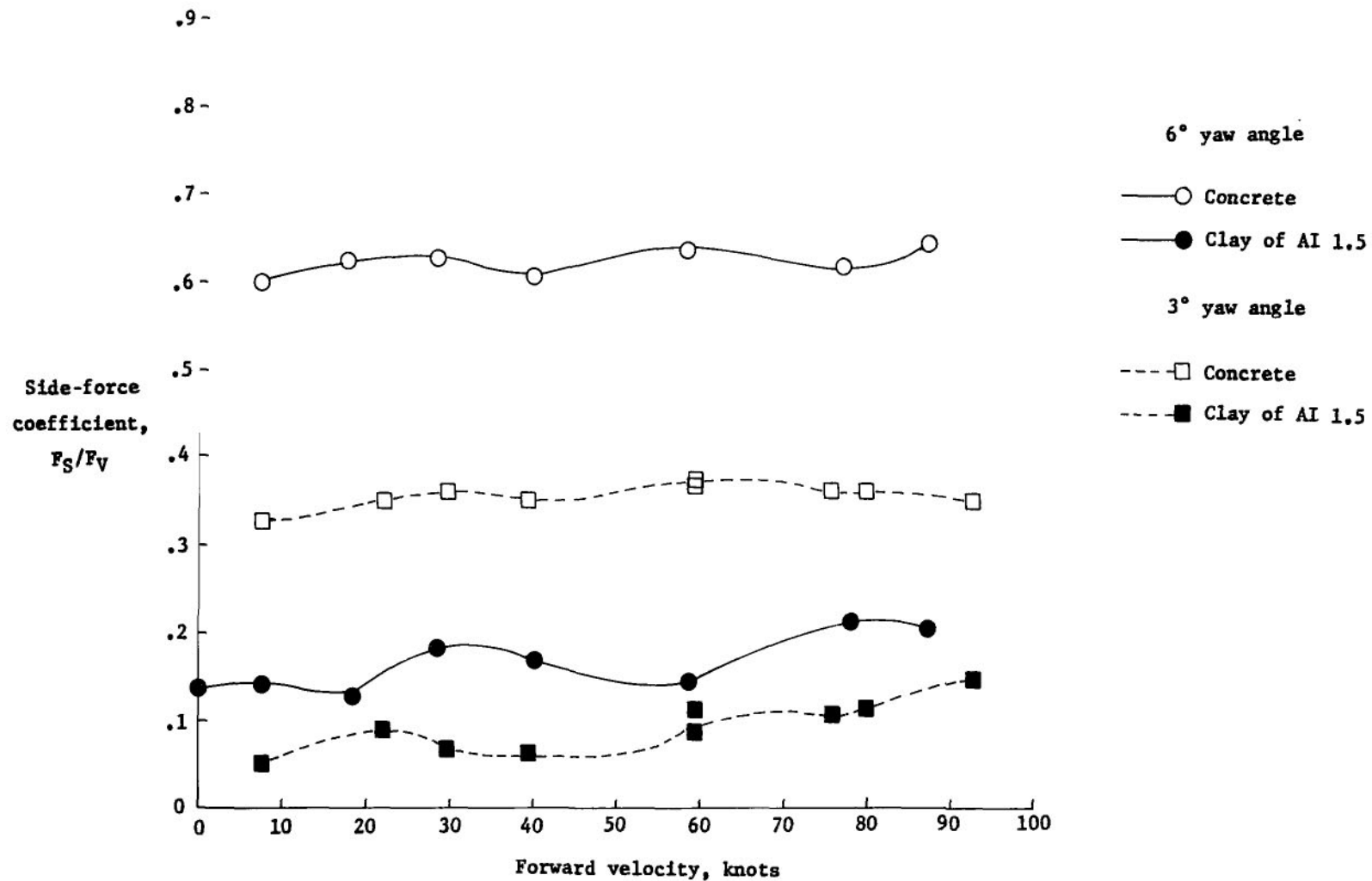
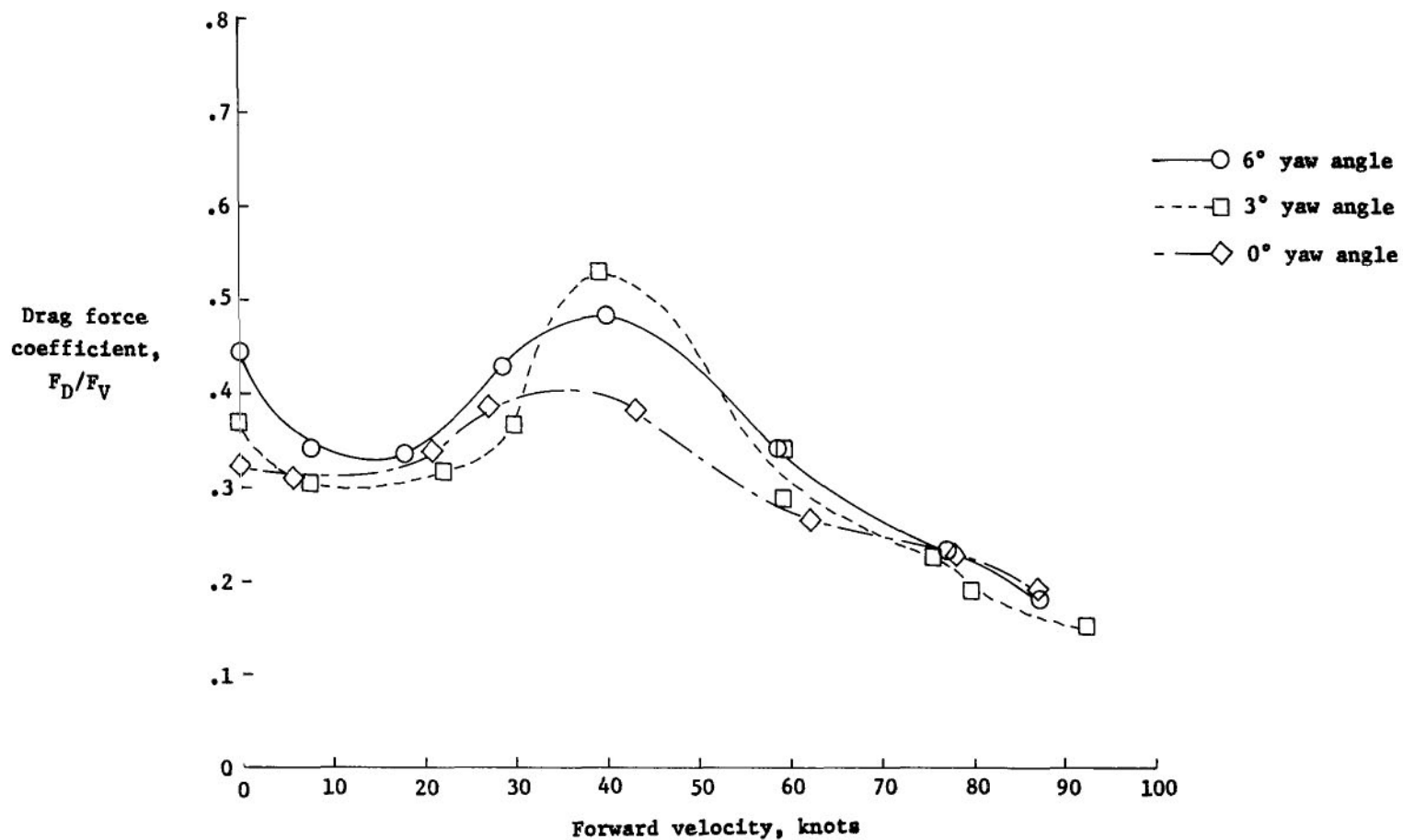


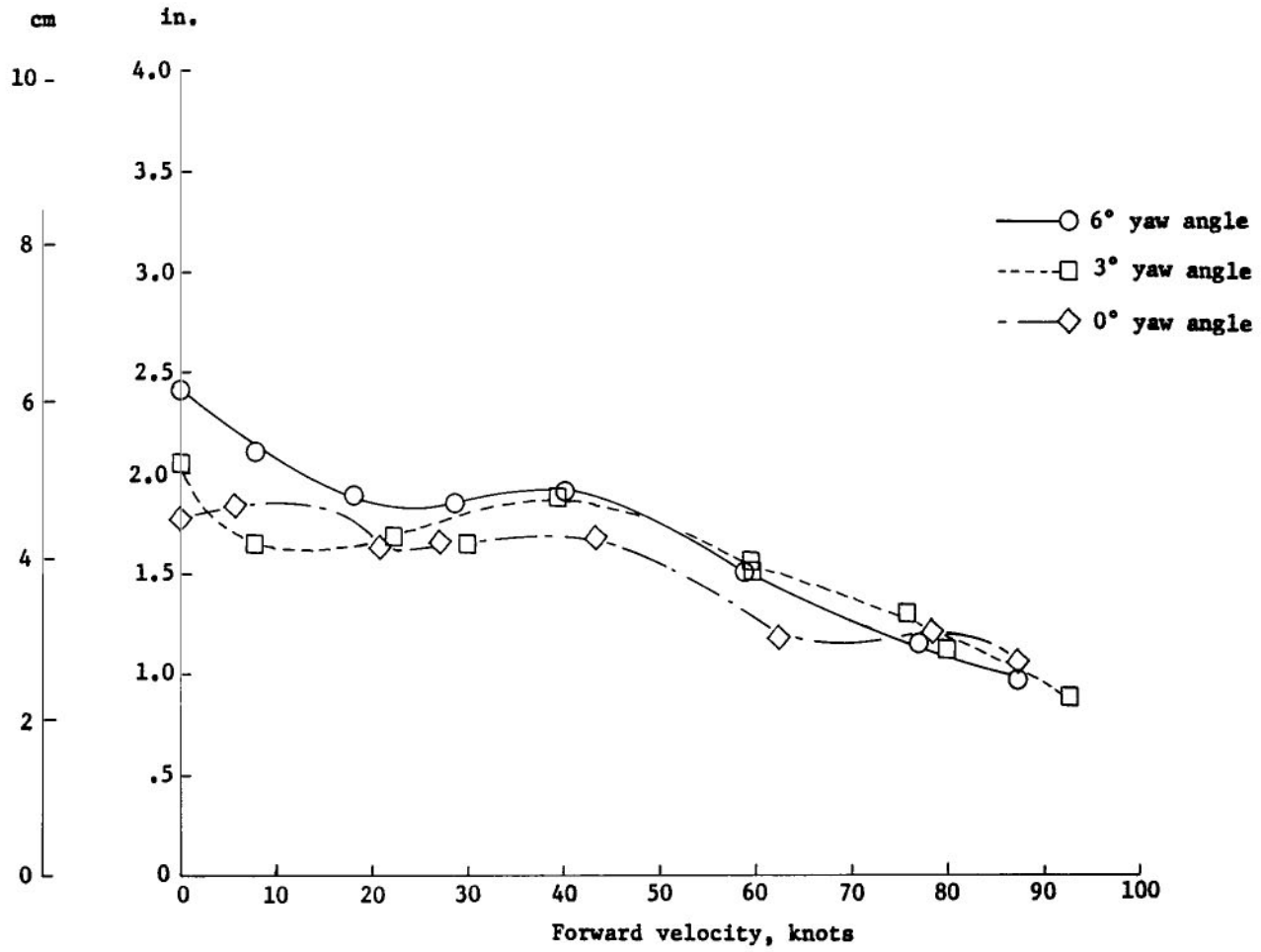
Figure 29.- Side-force coefficients developed by tire on concrete and on AI 1.5 clay at two yaw angles. SWDYN; $p_t = 48 \text{ N/cm}^2$ (70 lb/in²).



(a) Drag force coefficient.

Figure 30.- Drag force coefficients and rut depths developed in AI 1.5 clay by SWDYN during free rolling at 0° , 3° , and 6° yaw angles. $p_t = 48 \text{ N/cm}^2$ (70 lb/in²).

Average rut depth, z



(b) Rut depths.

Figure 30.- Concluded.

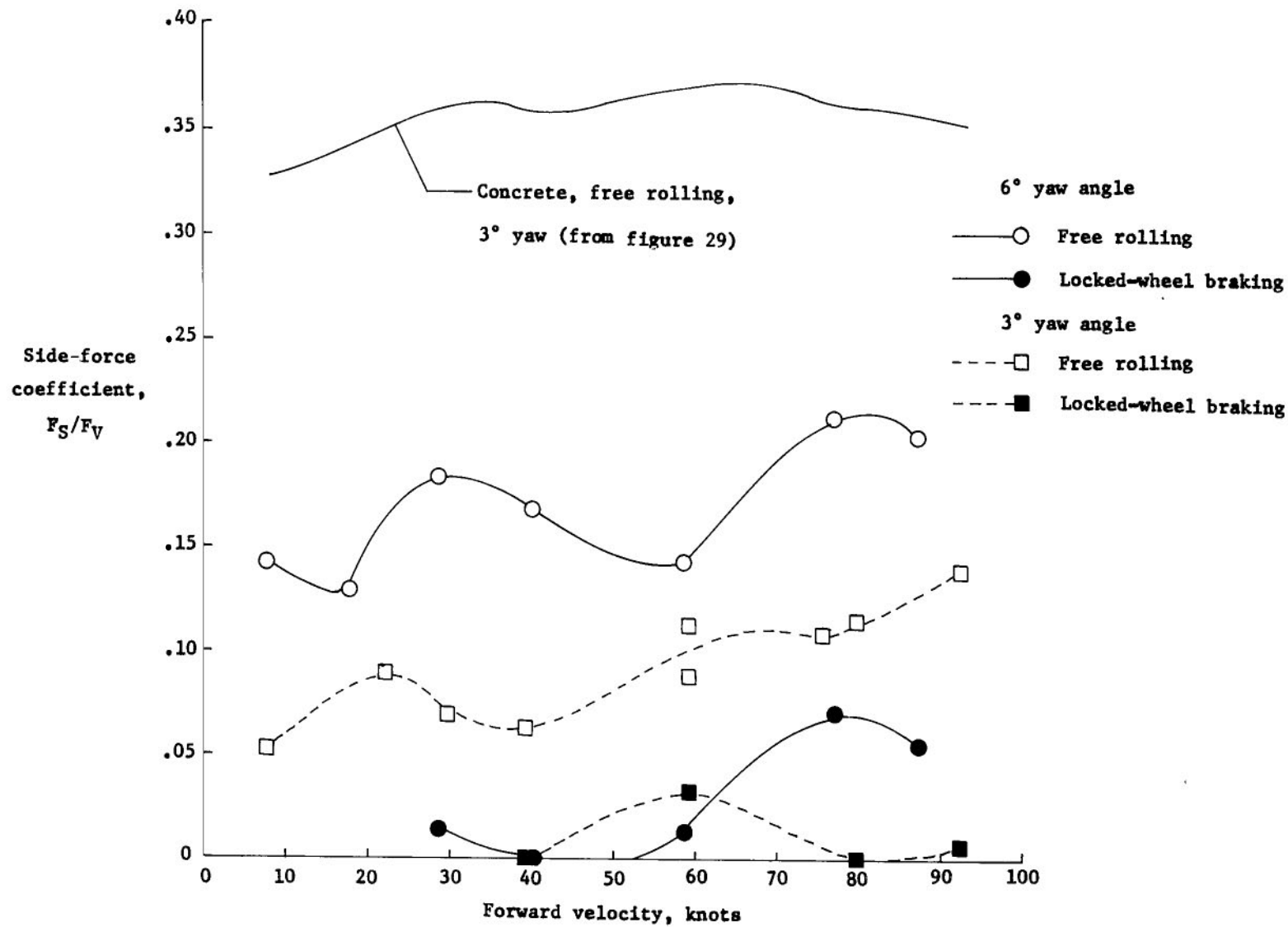


Figure 31.- Comparison of side-force coefficients developed by SWDYN during free rolling and locked-wheel braking. AI 1.5 clay; $p_t = 48 \text{ N/cm}^2$ (70 lb/in²).

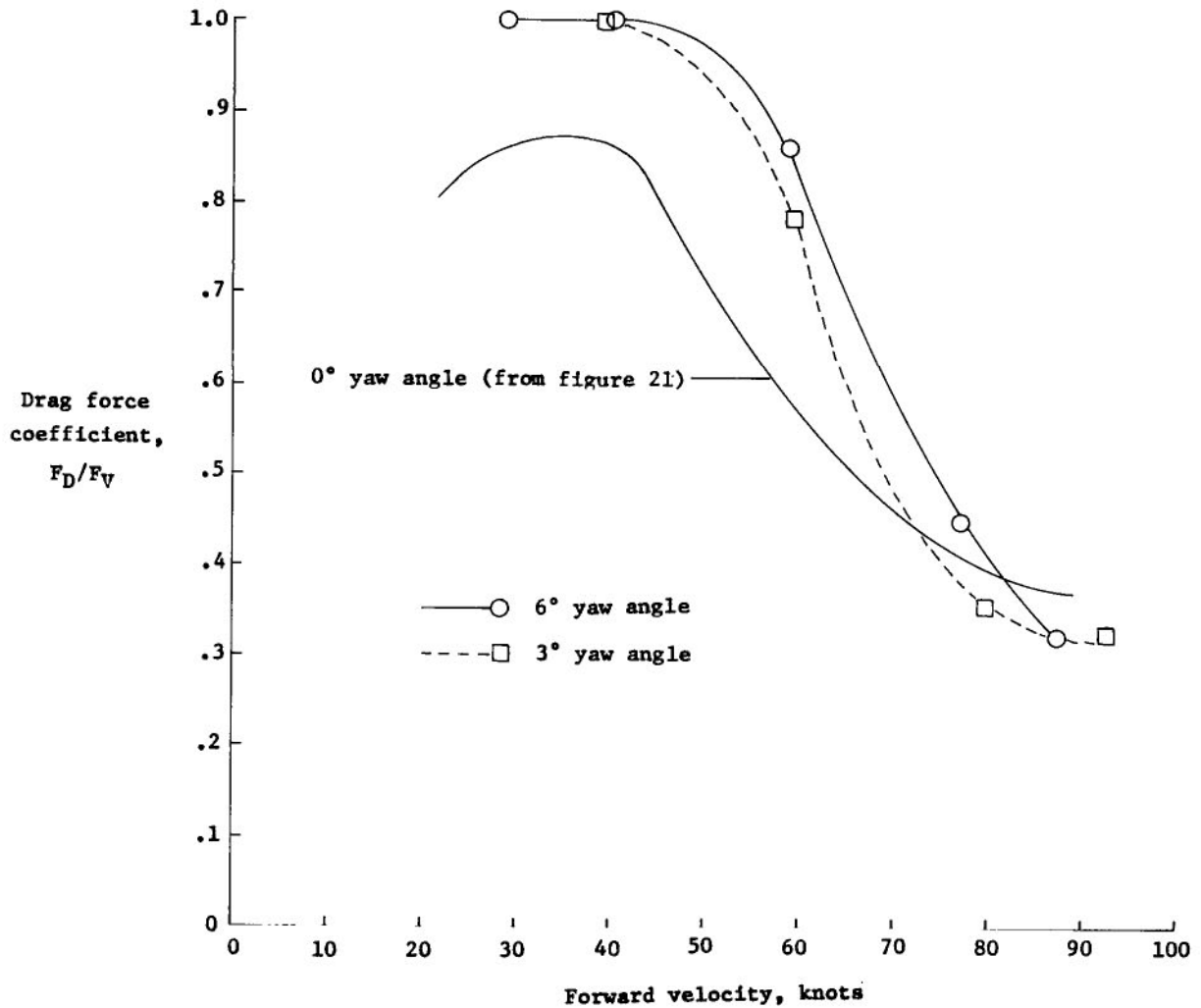


Figure 32.- Drag force coefficients developed by SWDYN during locked-wheel braking at 0°, 3°, and 6° yaw angles. AI 1.5 clay; $p_t = 48 \text{ N/cm}^2$ (70 lb/in²).

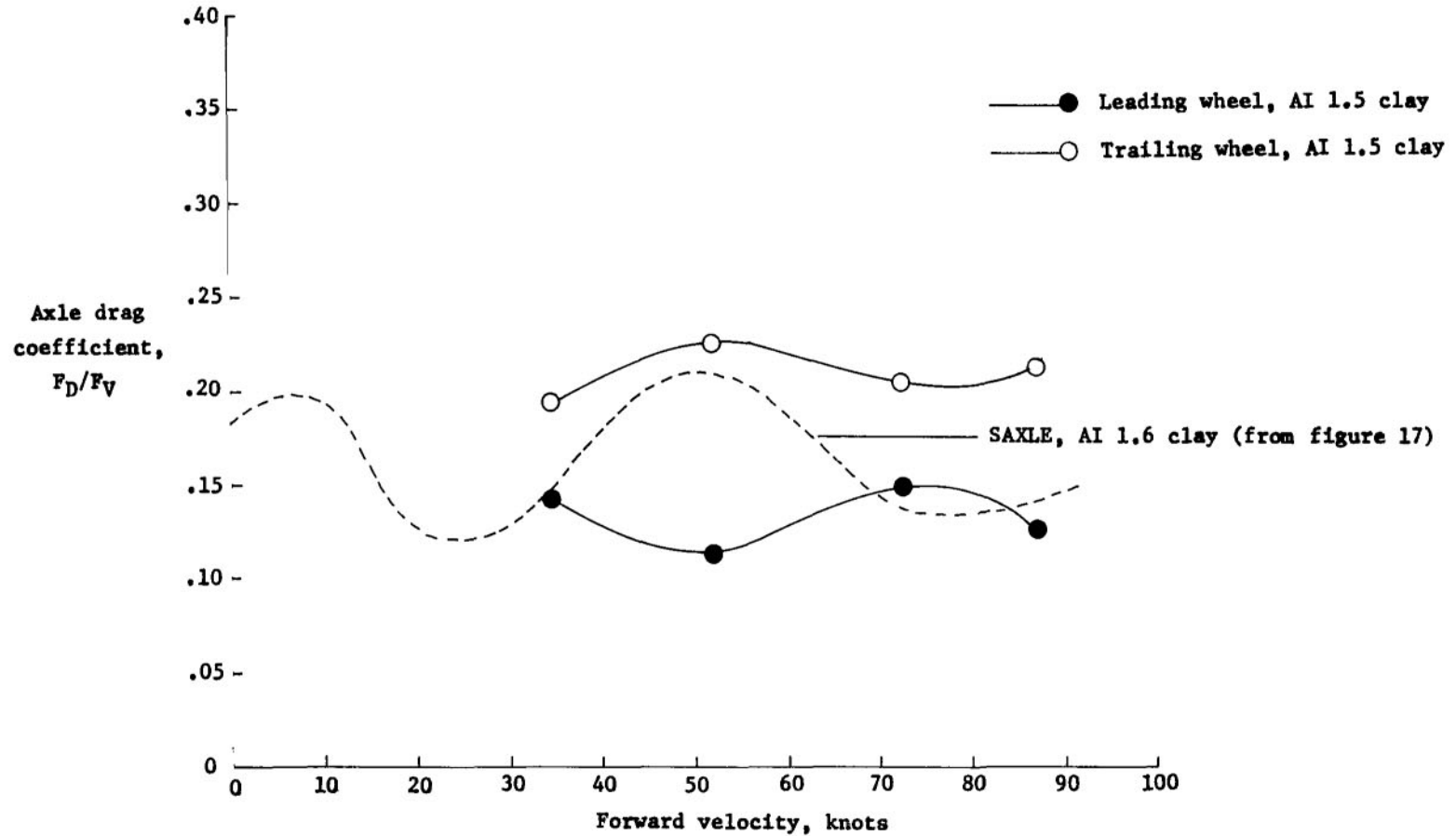


Figure 33.- Comparison of axle drag coefficients of a single wheel with each wheel in a tandem pair.
 $p_t = 21 \text{ N/cm}^2$ (30 lb/in²); $F_V \approx 22 \text{ kN}$ (5000 lb) per wheel.

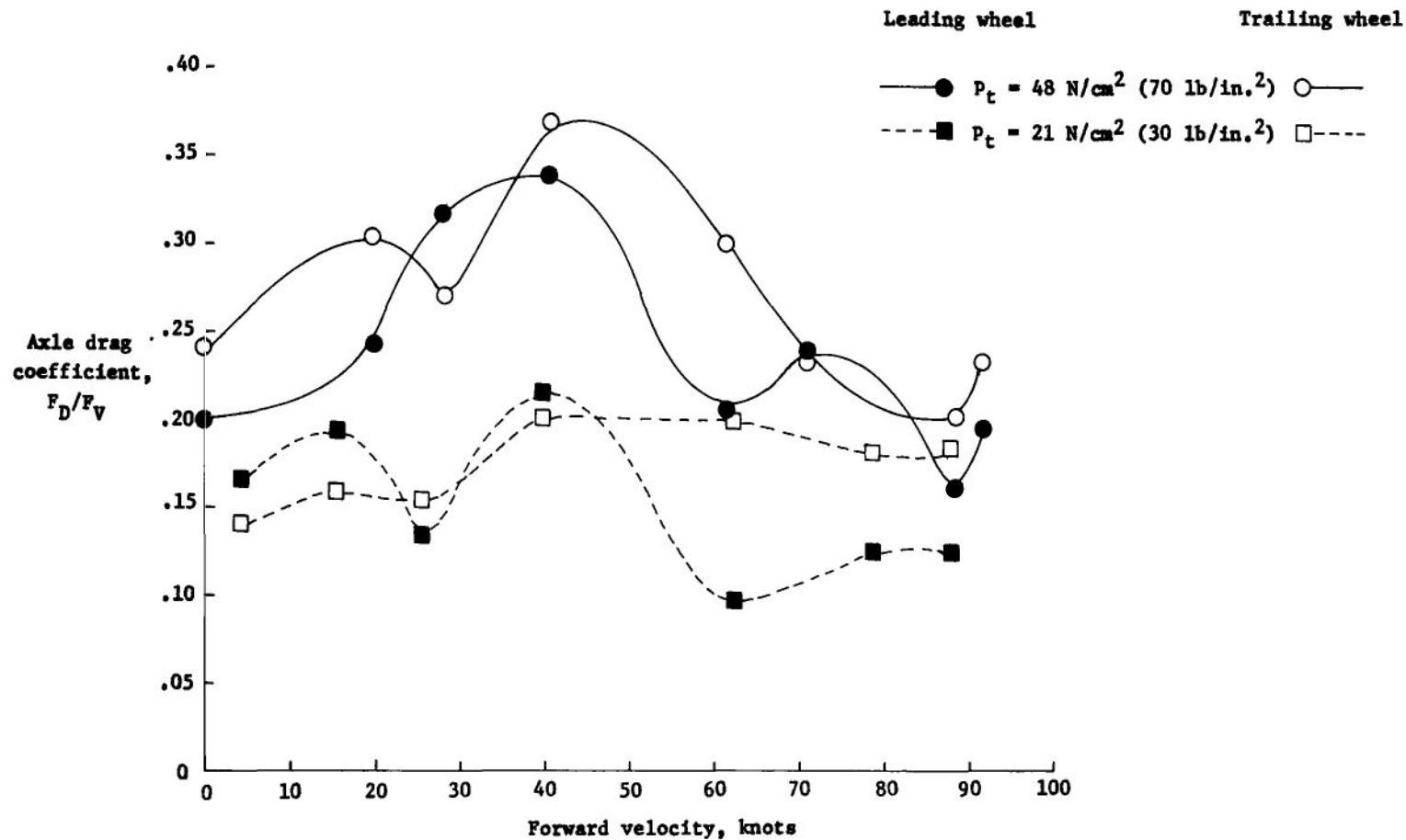


Figure 34.- Axle drag coefficients for tire operating in AI 1.5 clay. Each axle in a tandem pair; $F_V \approx 11 \text{ kN}$ (2500 lb) per wheel.

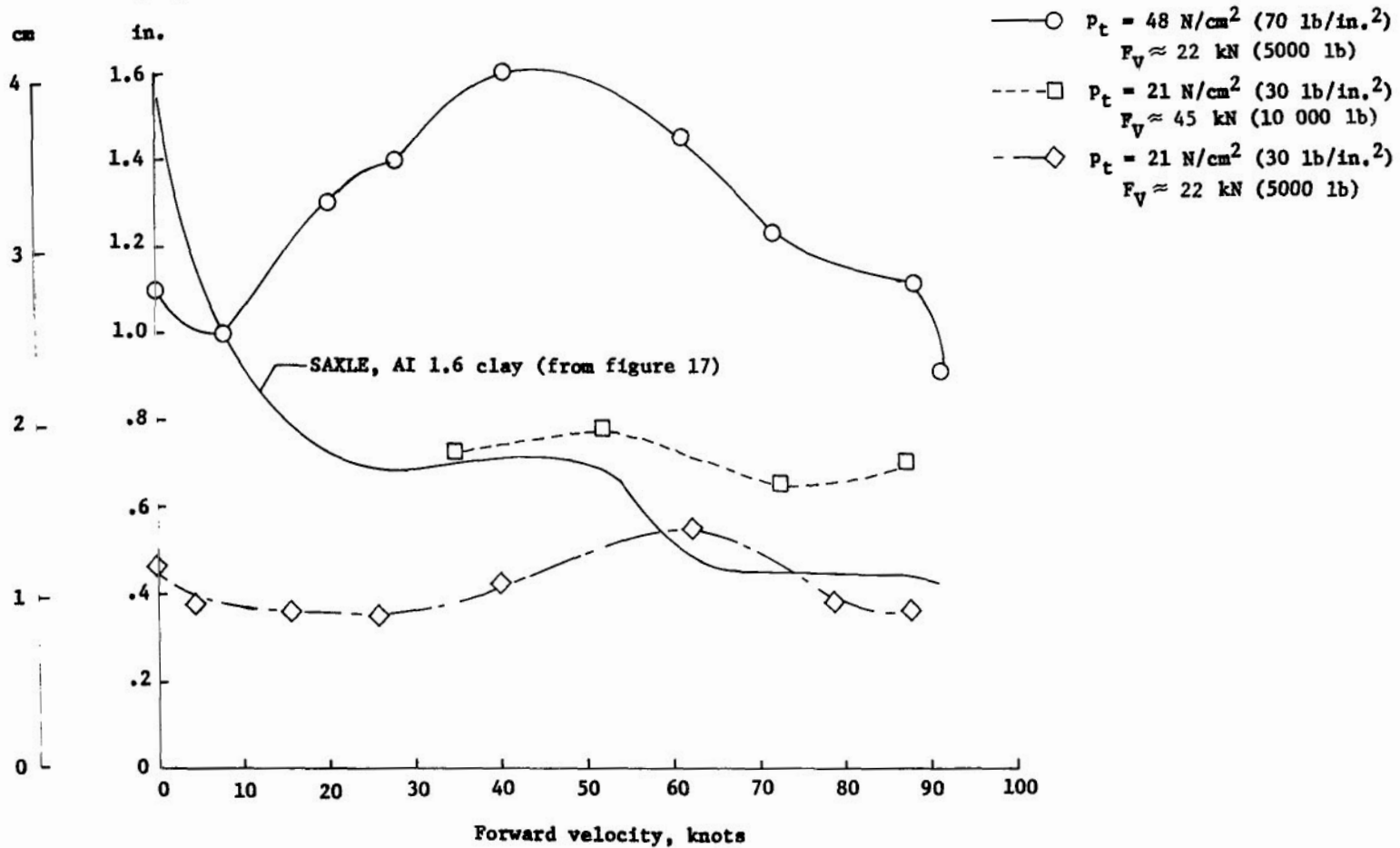
Average rut depth, z 

Figure 35.- Rut depths in AI 1.5 clay resulting from passage of tandem wheels.



012 001 C1 U 02 720721 SC0903DS
DEPT OF THE AIR FORCE
AF WEAPONS LAB (AFSC)
TECHNICAL LIBRARY/DCUL/
ATTN: E LOU BOWMAN, CHIEF
KIRTLAND AFB NM 87117

POSTMASTER: If Undeliverable (Section 158
Postal Manual) Do Not Return

"The aeronautical and space activities of the United States shall be conducted so as to contribute . . . to the expansion of human knowledge of phenomena in the atmosphere and space. The Administration shall provide for the widest practicable and appropriate dissemination of information concerning its activities and the results thereof."

— NATIONAL AERONAUTICS AND SPACE ACT OF 1958

NASA SCIENTIFIC AND TECHNICAL PUBLICATIONS

TECHNICAL REPORTS: Scientific and technical information considered important, complete, and a lasting contribution to existing knowledge.

TECHNICAL NOTES: Information less broad in scope but nevertheless of importance as a contribution to existing knowledge.

TECHNICAL MEMORANDUMS: Information receiving limited distribution because of preliminary data, security classification, or other reasons.

CONTRACTOR REPORTS: Scientific and technical information generated under a NASA contract or grant and considered an important contribution to existing knowledge.

TECHNICAL TRANSLATIONS: Information published in a foreign language considered to merit NASA distribution in English.

SPECIAL PUBLICATIONS: Information derived from or of value to NASA activities. Publications include conference proceedings, monographs, data compilations, handbooks, sourcebooks, and special bibliographies.

TECHNOLOGY UTILIZATION PUBLICATIONS: Information on technology used by NASA that may be of particular interest in commercial and other non-aerospace applications. Publications include Tech Briefs, Technology Utilization Reports and Technology Surveys.

Details on the availability of these publications may be obtained from:

SCIENTIFIC AND TECHNICAL INFORMATION OFFICE

NATIONAL AERONAUTICS AND SPACE ADMINISTRATION

Washington, D.C. 20546